Journal of Alloys and Compounds 885 (2021) 160939

Contents lists available at ScienceDirect

Journal of Alloys and Compounds

journal homepage: www.elsevier.com/locate/jalcom

Impact of TiO_2 on radiation shielding competencies and structural, physical and optical properties of CeO_2–PbO–B_2O_3 glasses

Gurinder Pal Singh[a,*], Joga Singh[a], Parvinder Kaur[a], Taminder Singh[a], Ravneet Kaur[b], Simranpreet Kaur[c], D.P. Singh[c]

[a] P.G. Department of Physics, Khalsa College, Amritsar 143002, India
[b] P.G. Department of Physics, Lyallpur Khalsa College, Jalandhar 144001, India
[c] Department of Physics, Guru Nanak Dev University, Amritsar 143005, India

ARTICLE INFO

Article history:
Received 8 May 2021
Received in revised form 18 June 2021
Accepted 21 June 2021
Available online 24 June 2021

Keywords:
Radiation Shielding
TiO_2 Glasses
CeO_2
Optical Properties
Elastic Constant

ABSTRACT

The glasses of series $xTiO_2$-$xCeO_2$-(30-x) PbO-(70-x) B_2O_3 where 2 ≤x ≤ 10 mol% were made using conventional melt-quench method and X-ray diffraction technique has been used to ascertain the amorphous nature of these glasses. The analysis of the compositional dependence of the physical parameters like density, molar volume and oxygen packing density along with the elastic parameters (Young's modulus, shear modulus, Vickers hardness number) of the studied glasses has been done. Infrared (IR) spectra revealed BO_3 and BO_4 units as main glass forming groups in these glasses but at higher concentrations of TiO_2, Ti^{3+} and Ti^{4+} ions get significantly incorporated in glass matrix thereby creating TiO_4 and TiO_6 structural units. Optical spectral studies indicated that the band gap energy values decreased with increasing TiO_2 content and these glasses had good UV-blocking efficiency which could be exploited for their use as transparent UV shielding materials. The radiation shielding parameters such as Half Value Layer, Linear Attenuation Coefficient, Exposure Buildup Factor, Mean Free Path including thermal and fast neutron cross section were deduced which indicated that the attenuation performance of these glasses improved with the addition of TiO_2. Lower values of Exposure Buildup Factor and higher values of thermal and fast neutron removal cross section reflect the proficient shielding ability of these glasses.

1. Introduction

The continuous growth in different industries and technologies demands utilization of more and more ionizing radiations. The ionizing radiation has great importance from the past era as they have potential applications in various fields like telecommunication, nuclear accelerator medical diagnosis and treatment, food preservation industry, space technology [1–6] etc. The manpower working in these industries with radiation appliances is daily exposed to different types of radiations and is facing enormous risk to their life. Among these radiations, gamma rays, due to zero mass and charge have the maximum penetrating power. So, the longer exposure to gamma radiations on humans can damage physical (cellular structure) and biological structure (genetic structure) leading to serious ailments like cancer [7–9]. For the safety and protection from these harmful gamma radiation exposures, many researchers have fabricated various kinds of shielding materials in the past [10–12]. One such material fabricated is concrete; which is used in many industries/ nuclear research centres for the safety of workers from the harmful exposure of these radiations. But due to some drawbacks of concretes like immovability/replacement, opacity and effect of water [13,14], it is less preferred presently and is replaced by more advantageous materials. More attention to glasses has been given as gamma-ray shielding materials due of their low cost, easy fabrication in a huge range of sizes of any form varying from optical fibres to glass windows [15–22], lightweight and thus easy movement or replacement, good mechanical strength and above all high transparency. In addition, glasses are more sustainable alternatives to lead when it comes to radiation shielding, as lead is highly toxic [23,24]. These properties are sufficient to say that glasses are possible contestants for their applications in gamma ray protection [23,24].

In particular, borate glasses were extensively considered in past era for diverse technological applications [25–27] because of their exceptional glass forming ability, high optical transparency, excellent radiation and thermal stability, interesting linear and

* Corresponding author.
E-mail address: gp_physics96@yahoo.co.in (G.P. Singh).

https://doi.org/10.1016/j.jallcom.2021.160939
0925-8388/

nonlinear optical properties and good solubility of rare-earth (RE) or transition metal (TM) elements [28–30].

In glass matrix, role of transition metal ions has been widely studied because their presence helps to modify various properties of glasses namely electrical, optical, physical and structural properties [31–33]. The metals possessing wide band gap like zinc, tungsten, and cerium have been surveyed as fabulous radiation protecting materials [34–36]. Among transition metal oxides (TMO), titanium oxide (TiO_2) has been utilized in enhancing the optical properties of glasses [37–43]. It more often exists in electronic states Ti^{4+} and Ti^{3+} in glass matrix [44–46]. TiO_2 cannot make glass itself but since it acts as a modifier, it is used in many glass compositions [47]. The occurrence of minute quantities of TiO_2 within the glass environment boosts the glass making capability and chemical durability of glasses [48,49]. In titanium, the unfilled D-shells contribute extensively to the non-linear polarizability; consequently titanium based borate glasses are highly capable materials to be exploited as nonlinear optical devices. Recently, titanium based materials are used in some promising applications like efficiency enhancement of silicon solar cells [50], radiation protection [9], bioactive glasses [51], DSSC (Dye-Sensitized Solar Cells) [52] and UV radiation protection and as sunscreens [53].

Among RE metals, cerium doped oxide glasses are very useful because of their existence in two stable states Ce^{3+} and Ce^{4+} in glasses. Consequently, the investigated glasses have optical and lasing properties in near UV or visible and infrared region. These glasses are highly capable to absorb UV-radiation which also shows that in the visible light range, these have high transparency [35,54–56]. Use of Cerium based glasses as brighter scintillation materials under X-ray irradiation has also been reported [57].

However, the gamma ray shielding properties of titanium and cerium doped glasses have been described by few studies [14,46,54,58]. In light of this, five glass samples with composition $xTiO_2$-$xCeO_2$-(30-x)PbO-(70-x)B_2O_3 (where with 2 ≤x ≤ 10 mol%) were fabricated. The hypothesis is to examine the positive impact of adding TiO_2 in CeO_2-PbO-B_2O_3 glasses on the radiation shielding competencies as well as structural, physical and optical properties of these glasses. This is expected to increase their radiation hardness and stability; henceforth making them eligible candidates to be used in radiative environments.

The structural and optical properties were determined using XRD, FTIR, and UV–visible measurements. Various shielding parameters such as Linear Attenuation Coefficient (μ), Half Value Layer (HVL), Mean Free Path (MFP), Exposure Buildup Factor (EBF) and Fast/Thermal neutron cross section have been evaluated to find out most effective glass composition for protection against gamma-rays. The outcome of the prepared glasses on comparing with different concretes unquestionably indicated the dependence of these parameters on the incident photon energy and chemical composition of the glass samples. The T5 glass sample having high density emerges as the most effective shield and might be helpful in the construction of active shielding against hazardous gamma radiation. The authors believe that the aftermaths of the presented work will be advantageous for understanding the direct impact of TiO_2 on the structural, optical, physical and nuclear radiation shielding properties of cerium borate glasses.

2. Experimental procedure

2.1. Preparation of glasses

The glasses with formula $xTiO_2$-$xCeO_2$-(30-x)PbO-(70-x) B_2O_3 with 2 ≤x ≤ 10 mol% are prepared with the help of melt quenching technique. The necessary mixture of chemicals mentioned in Table 1 is grinded to get a fine powder and is melted in a silica crucible at a temperature of 1100–1200 °C for 60 min until a homogenous bubble-free liquid is formed. The melt is poured into a preheated steel mould and annealed at a temperature of 390 °C for 1 h to secure against the breaking of the sample by residual internal strains [59,60]. The samples are polished with cerium oxide to obtain maximum flatness. The prepared glasses with composition are tabulated in Table 1. In the present investigation, the experimental techniques are same as deployed in our earlier work [59,60]. The physical appearance of glasses is shown in Fig. 1.

Table 1
Nominal composition of glasses (mole %).

Glass	TiO_2 (%)	CeO_2 (%)	PbO (%)	B_2O_3 (%)
T1	2	2	28	68
T2	4	4	26	66
T3	6	6	24	64
T4	8	8	22	62
T5	10	10	20	60

Fig. 1. TiO_2–CeO_2–PbO-B_2O_3 glass samples.

3. Results and discussion

3.1. X-ray diffraction

As depicted from X-ray diffractograms of TiO_2 doped CeO_2–PbO–B_2O_3 glasses (Fig. 2), not any of the prepared samples displayed sharp crystalline peaks. The attribution to the fact that concentration of crystalline phases is not present in prepared glasses reflects the characteristics of amorphous structure. A broad hump was observed for all samples at 2θ ~28° – 30° confirming that there does not exist any long-range atomic order confirming their amorphous structure. Similar observations have also been made by many researchers [24,61]. The enhancement in the TiO_2 concentration substitution proportion did not disturb the amorphous nature of the glass samples. So, we can make clear observation that prepared samples are far from crystallinity and have amorphous structure.

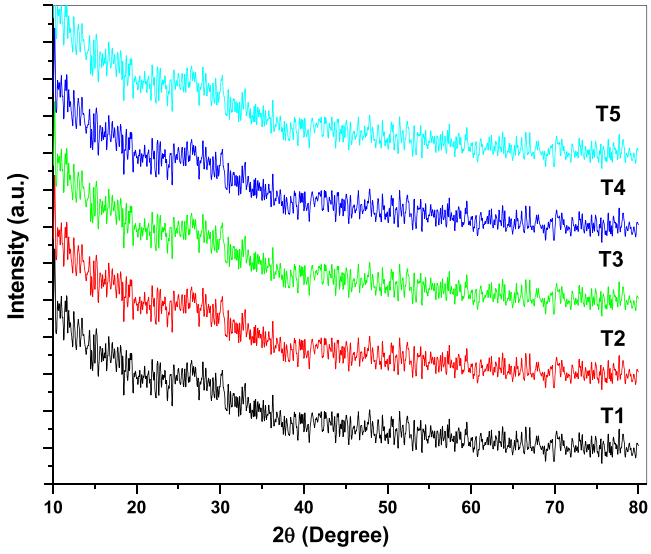

Fig. 2. X -Ray diffraction pattern of TiO_2–CeO_2–PbO–B_2O_3 glasses.

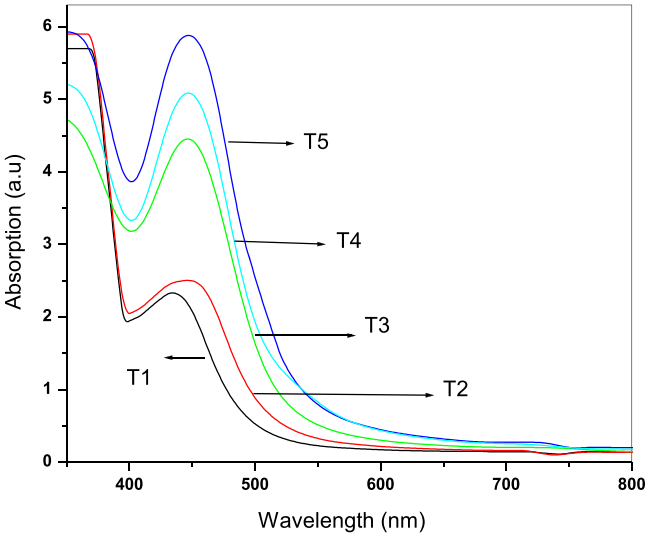

Fig. 3. Optical Absorption of TiO_2–CeO_2–PbO–B_2O_3 glasses.

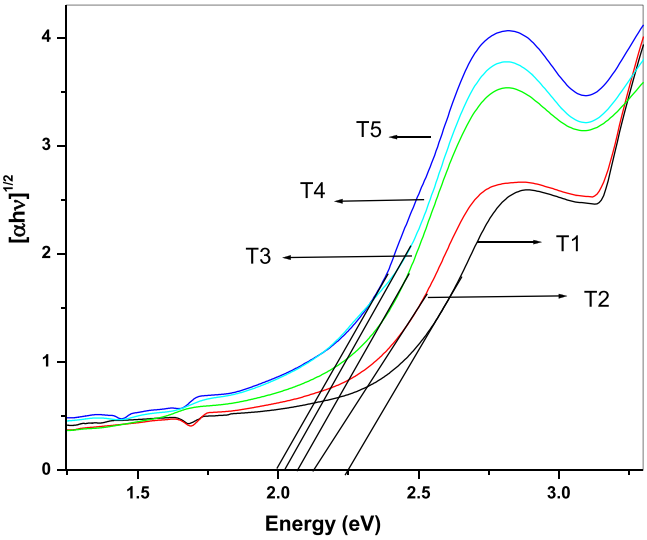

Fig. 4. Band gap of TiO_2–CeO_2–PbO–B_2O_3 glasses.

3.2. Optical properties

To explore the UV-shielding capability of samples, UV-Vis absorption spectra of T1-T5 samples are presented in Fig. 3. As compared to T1 and T2 samples, a strong UV-shielding effect is observed in T3–T5 samples. At the same time, all visible light has not been absorbed by these samples. Absorption spectrum indicates that all glass samples have optical absorption beyond the 400 nm i.e in visible region. The absorption edge shifts to a longer wavelength from T1 to T5 samples. The band edge shifts from 439 to 595 nm in sample T1, from 449 to 610 nm in sample T2 and from 449 to 663 nm in samples T3 to T5. But in our previous study of CeO_2–PbO–B_2O_3 glasses, band edge shifted from 334 to 469 nm [59]. This large shift in band edge happens only due to presence of TiO_2 that played effective role to alter the glasses network so that band edge gets shifted more towards the longer wavelength as compared to incorporation of cerium addition in glass samples.

It is a proven fact that titanium exists primarily in Ti^{4+} state in the glass network. On the other hand, during the process of melting of the glasses, there may be a possibility of reduction of Ti^{4+} ions into Ti^{3+} ions [51–53,62]. The band observed in the optical absorption spectra at about 480 nm of the studied glasses is identified as being due to $2B_{2g} \rightarrow 2B_{1g}$ octahedral transitions of the Ti^{3+} ($3d^1$) ions [62] which were missing in our previous studies of CeO_2-PbO-B_2O_3 glasses. This band is growing in glasses samples T4-T5 at high concentration of TiO_2 which indicates the increase in number of Ti^{3+} ions at the expense of reduction of Ti^{4+} ions [62–66].

To determine the band gap, absorption coefficient (α), Planck's constant (h) and frequency (ν) are used which are relatively expressed in the Urbach plots between $(\alpha h\nu)^{½}$ and energy (hν) of TiO_2–CeO_2–PbO–B_2O_3 as shown in Fig. 4 [59,60]. As depicted in Table 2, the optical band gap energy of glasses declined due to presence of titanium. Many factors are accountable for this red shift in absorption edge and shrinkage in the energy band gap.

First factor of this amendment in band energy is the configuration of tetrahedral BO_4 units in glass network. These BO_4 units are proficient to formulate more strongly bonded glass network and also these BO_4 groups are denser than trigonal BO_3 groups because the bond strength of B–O (808.7 kcal/mol) > Ce–O (795 kcal/mol) > Ti-O (672 kcal/mol) > Pb–O (382 kcal/mol) which results in the decrease in optical band gap [60]. Therefore these tetrahedral units of borate are responsible for reduction in the band energy along with change of absorption edge on longer wavelength side which results in forming more stable glasses structures [60].

At higher concentration of TiO_2, the change in band gap energy is seen which is due to growth in the fraction of network forming Ti^{3+} ions and it may prominently act as a modifier in the glass network. Usually, the higher concentration of Ti^{3+} in the glass host creates more donor centers which results in the creation of negatively charged electrons [64,66,67]. One cause of reduction in the proportion of Ti^{4+} ions in the glass network is creation of donor center [66,67]. This progression shifted its absorption edge towards the longer wave number and thus the value of the optical band gap energy decreases [67].

One more factor accountable for this red shift is the easily oxidizing nature of Ce^{3+} ions to Ce^{4+} ions because of their electron donor ability i.e $Ce^{3+} \rightarrow Ce^{4+} + e^-$ [60,68].

Fajan and Kreidle have given a rule that the polarizing power of cation enhances on diminishing its size and increasing its positive charge. As the ionic radius of cations Ti^{4+}, $Ce^{4+}$and Pb^{2+} are 0.64 Å, 1.02 Å and 1.32 Å respectively i.e ionic radius of $Pb^{2+} > Ce^{4+} > Ti^{4+}$, therefore, the cation polarizability of titanium is greater than other components of glasses [69,70]. This factor causes shifting of the absorption edge to the larger wavelength side which results in reduction of the band gap [70].

The UV-Vis transmission spectra of T1–T5 samples are presented in Fig. 5. All samples indicate visible light transmittance at 400–800 nm. It is significantly revealing that the transmittance of all samples in the UV region from 200 to 380 nm is zero which is worthwhile for applying in UV-shielding devices [14,46]. Hence these glasses have full-band UV-shielding ability.

Additionally, Transmittance simultaneously gets reduced with an increase of TiO_2. This behaviour could be related to the lot of defect energy levels present inside the optical band gap energy level [71,72].

Refractive index of a glass is a vital tool to determine any change in its structure due to variation in glass system's composition. In the present study, we observe that on replacement of borate oxide by high atomic mass, high field strength TiO_2, the refractive index increases from 2.64 to 2.74 (Table 2). The reason for this is the defect energy levels introduced by network metal oxide [73,74]. As pointed out above that diminishing the fraction of network forming Ti^{4+} ions in the glass system continuously leads to an enhancement in the creation of donor centres resulting in an escalating overlap between empty 3d states of Ti^{4+} sites and the nearby excited states of circumscribed electrons that

Table 2
Optical properties of glasses.

Glass	Optical Band Gap ($E_{opt.}$) (eV)	Refractive Index	Electronic polarizability (Å^3)	Theoretical Optical Basicity	TPA
T1	2.25	2.64	2.956	1.398	18.54
T2	2.19	2.66	2.970	1.406	19.02
T3	2.13	2.68	2.985	1.414	19.51
T4	2.02	2.73	3.011	1.429	20.40
T5	2.00	2.74	3.016	1.431	20.56

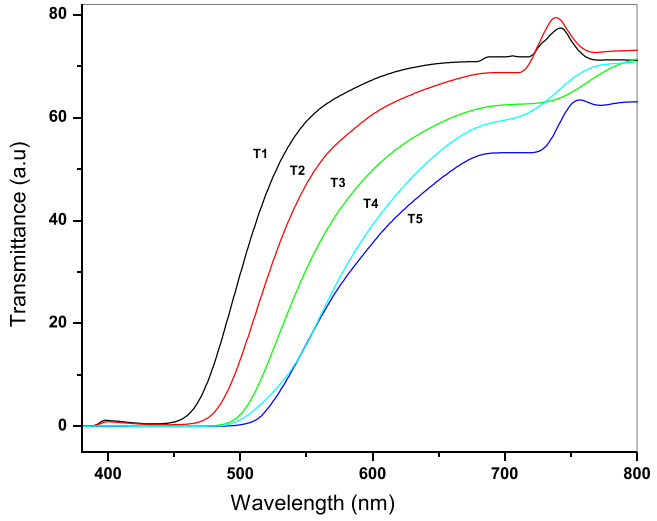

Fig. 5. Transmittance of TiO_2–CeO_2–PbO–B_2O_3 glasses.

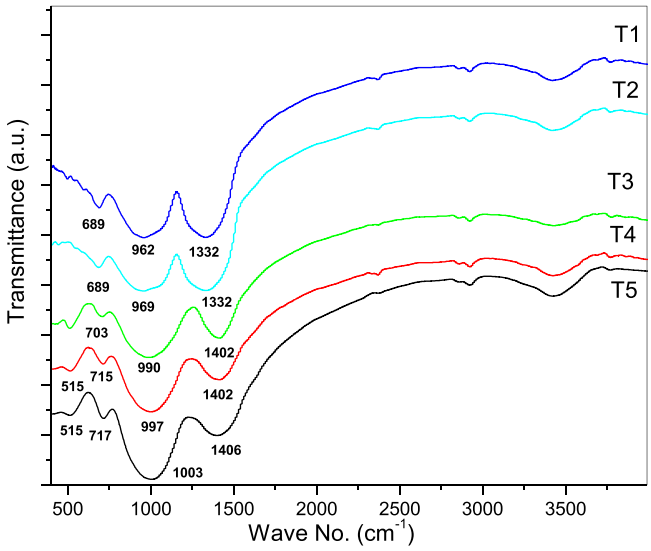

Fig. 6. FTIR spectra of TiO_2–CeO_2–PbO–B_2O_3 glasses.

were trapped originally on Ti^{3+} ions [40]. Such overlap is one more cause for enhancement in refractive index.

This increase in refractive index may also be explained with the help of optical basicity (OB) of glass constituents. According to V. Dimitrov and T. Komatsu, the values of optical basicity of each oxide are: ΛTiO_2 0.96 > ΛCeO_2 0.65 > Λ B_2O_3 0.42 [74]. The values indicate that titanium has greater values of OB than other elements in glass sample resulting in an enhancement in refractive index of the glasses [75].

3.3. Theoretical optical basicity and electronic polarizability

The optical basicity of glasses gets altered with the presence of oxygen ions available in the glasses network which creates of negative charges. Optical Basicity depends on the basicity of different metal oxides present during the creation of glasses.

The theoretical optical basicity (Λ_{Th}) and electronic polarizability (α_e) are determined using the expression [68,75,76].

Theoretical Optical Basicity $(\Lambda_{th}) = -\chi^*0.5 + 1.7$.

Electronic polarizability $(\alpha_e) = -0.9^*\chi + 3.5$ where electronegativity $(\chi) = 0.2688\ E_g$.

It is calculated that as the content of TiO_2 increases, correspondingly its theoretical optical basicity and electronic polarizability get increased (Table 2). Here it is confirmed that the increased value of optical basicity revealed the capability of oxide ions to transfer electrons to the nearby surrounding cations. So, one more factor is that these results are in support of donor centres formation. This is one of the causes of the shift in absorption edge and decline in band gap [68].

3.4. Two-photon absorption coefficient

To search about the ability of these glasses to have some solid state photonic applications, TPA (two-photon absorption coefficient) is very important tool. It is obtained by using the subsequent equation [77].

Two Photon Absorption Coefficient $\beta(cm/GW) = [36.76 - 8.1E_g]$where E_g is optical band gap.

The TPA of the glasses is increasing gradually from 18.54 to 20.56 with the inclusion of titanium oxide as given in Table 2. Here it indicates that these glasses may be useful in some photonic devices.

3.5. FTIR (Fourier Transform Infrared Spectroscopy)

The FTIR spectra of titanium oxide doped CeO_2–PbO–B_2O_3 glasses in 400–4000 cm^{-1} region with TiO_2 concentration 2–10 mol% are illustrated in Fig. 6. FTIR spectra of the borate glasses are generally characterized by three fundamental absorption bands. The first region lies around 600–700 cm^{-1} due to the bending of B–O–B linkages of the BO_3 group. The second region ranges from 800 to 1200 cm^{-1} because of B–O stretching of tetrahedral [BO_4] units of borate. The third region located among 1200–1600 cm^{-1} is because of the B–O stretching of [BO_3] units [78–81].

1. In the FTIR spectrum, origin of a band at 515 cm^{-1} in T3 glass sample is due to presence of vibration of Ti–O bond in the TiO_6 octahedral structural units [82]. The intensity of this band is decreasing at a higher concentration of titanium oxide in samples T4 and T5. One thing to be noted here is that this band was absent in our previous study of CeO_2–PbO–B_2O_3 glasses [59]. This indicates that titanium addition affects the structure of the studied glasses.
2. A small and sharp peak in sample T1 is observed at about 689 cm^{-1} which substantiates the existence of B–O–B bending vibration of [BO_3] groups. It is observed that intensity of this band increases in samples T3–T5 at mole percent (4–10%) of TiO_2 contents and also its position gets shifted towards the higher wave number (689–717 cm^{-1}). This behaviour comes up, when

vibration of B–O linkages is distorted in the glass network and also vibrations of B–O–Ti linkages of TiO_4 groups are present both at tetrahedral and octahedral positions in the glass network [62,82,83]. This reveals the alteration of borate network on adding titanium oxide.

3. The band present at 962 cm^{-1} in sample T1 is due to the occurrence of stretching vibrations of different tetrahedral [BO_4] units in tri, tetra and penta-borate groups [63,64]. When titanium oxide is incorporated (6–10 mol%), this band gets shifted towards the higher wave number (1009–1066 cm^{-1}) in T3 to T5 samples and its intensity also gets raised with an enhancement of TiO_2 contents [68,70]. This is due to the development of more BO_4 units in the glass matrix with the addition of titanium oxide.
4. In sample T1, band present at 1332 cm^{-1} is due to [BO_3] groups [63]. The intensity of this band gets reduced and its location is shifted to higher wave numbers in other samples [60,68]. Accordingly, the intensity of peak at 900–1000 cm^{-1} increases which indicates that more tetrahedral boron groups are formed in glass network at higher concentrations of titanium oxide.
5. It has been noticed that the higher concentration of TiO_2 helps to offer more oxygens which facilitates to alter the trigonal [BO_3] into [BO_4] groups and Ti^{+4} (tetrahedral and octahedral) and Ti^{3+} (only octahedral) groups of titanium are also formed [62,83,84].

3.6. Density and molar volume

The density and molar volume of prepared TiO_2–CeO_2–PbO–B_2O_3 glasses are given in Table 3. In our previous study the density of the cerium glasses got increased (3.34–3.99 g/cm^3) with an incorporation of cerium [59]. But now it is calculated that with an addition of TiO_2, there is greater increase in value of density from 3.35 to 4.21 g/cm^3. It is because of the increase of molecular weight with increase in the concentration of titanium in the glass system as B_2O_3 is replaced with TiO_2 having higher molecular mass (79.866 g/mol) than B_2O_3 (69.63 g/mol). One more reason for enhancement in density is the creation of more compact [BO_4] groups which arise because of the availability of more oxygens. Consequently, this factor alters BO_3 units into BO_4 [68,85]. The change of molar volume and density with increasing titanium oxide content is depicted in Fig. 7. The density has higher value in samples T3–T5, which is also due to the creation of B-O-Ti linkage in the borate system which strengthens the glass system [84].

The molar volume played an imperative role as it is observed in this system that decrease in the value of molar volume leads to a reduction in inter-atomic spacing or bond length which causes contraction of glass structure.

Contracting of glasses is established by the calculated value of average boron-boron separation $< d_{B\text{-}B} >$ [68,77,85].

Table 3
Physical parameters of glasses.

Sample Code	T1	T2	T3	T4	T5
Density (D) (g/cm^3)	3.35	3.44	3.68	3.89	4.21
Molar Vol. (cm^3/mol)	34.29	33.16	30.78	28.9	26.51
$< d_{bb} >$ (nm)	0.446	0.433	0.414	0.398	0.38
V_0	14.29	13.82	12.83	12.04	11.05
OPD	69.98	72.38	77.99	83.04	90.53
Average Coordination (m)	4.08	4.16	4.24	4.32	4.4
Bond density (n_b × 10^{29} m^{-3})	0.717	0.756	0.830	0.900	1.000
Average Molecular weight (M)	114.88	114.07	113.25	112.43	111.62
Number density: N (*10^{20} ions/cm^3)	3.51	7.27	11.74	16.67	22.72
Polaron radius (r_p) (Å)	1.23	0.966	0.823	0.732	0.604
Inter-nuclear distance (r_i) (Å)	3.05	2.4	2.04	1.82	1.64
Field Strength (F) (*10^{17}cm^{-2})	3.83	6.22	8.56	10.82	15.9

$$\text{Average boron} - \text{boron separation} < d_{B-B} > = \frac{V_m^B}{N_A}$$

where N_A is Avogadro number and $V_m^B = \frac{V_m}{2(1-X_B)}$, V_m is molar volume, X_B molar fraction of B_2O_3.

The value $< d_{B\text{-}B} >$ dwindles progressively with increase of TiO_2 contents. Thus, the existence of titanium ions facilitates to reduce the average boron-boron separation which shows the way to compaction of glass network. Consequently, there is change in molar volume and the density of glasses.

The oxygen packing density (OPD) and molar volume of oxygen are also calculated by the formula mentioned below [68,85].

$$\text{Oxygen packing density (OPD)} = 1000C\left(\frac{\rho}{M}\right)$$

$$\text{Molar volume of oxygen } (V_0) = \sum_i \frac{V_m}{x_i n_i}$$

The value of molar volume of oxygen and oxygen packing density are in opposite trends i.e decline in V_0 and enhancement in OPD shows that the structure of glass is tightly packed [as shown in Table 3] which is due to the presence of more bridging oxygen forms in the glass system [41,42]. These forms create a compact structure of glass.

The Ion concentration (N), inter-nuclear distance (r_i), polaron radius (r_p) and field strength (F) are estimated using the relations [68].

$$\text{Ion Concentration } (N) = \frac{Density\,(\rho) \times Avogadro\ No.\ (N_A) \times mole\%(RE)}{Average\ Molecular\ Weight\,(M)}$$

$$\text{Inter} - \text{nuclear distance } r_i(\text{Å}) = \left(\frac{1}{N}\right)^{1/3}$$

$$\text{Polaron radius } r_p(\text{Å}) = \frac{1}{2}\left(\frac{\Pi}{6N}\right)^{1/3}$$

$$\text{Field strength (F)} = \frac{Z}{r_P^2}$$

The calculated outcomes of inter-atomic distance, r_i, and concentration of ions, N, are listed in Table 3. It is seen that the inter-atomic distance decreases gradually from 3.05 Å to 1.64 Å and polaron radius decreases from 1.23 Å to 0.604 Å whereas the ions concentration (N) increases with enhancement of TiO_2 content. This decrease in r_i and r_p indicates the rise in compactness of glass matrix with the concentration of TiO_2. As observed from Table 3, the field strength enhances with enhancement of TiO_2 content. This boom in field strength is ascribed due to the lowering in inter-atomic distance, polaron radius and increase in value of BO_4 groups in glasses [68].

Increase in density and the resulting decrease in molar volume expose that titanium oxide acts as a modifier in these prepared glasses.

3.7. Packing density

The molar volume is utilized to find out an imperative parameter that helps to explain the atomic packing density of atoms (V_T) or atomic packing fraction (APF) and the compactness of glasses. APF or Packing density (V_T) is calculated by the equation mentioned below [85].

$$\text{Packing density } (V_T) = \sum \frac{V_i x_i}{V_m}$$

Table 4
Packing Density (V_T), Poisson ratio (σ), Young's Modulus of Elasticity (E), Modulus of Compressibility (K), Modulus of Elasticity in Shear (G) and Vickers Hardness Number (H) of the glass samples respectively.

Glass	Packing Density (V_T)	Poisson ratio (σ)	Young's Modulus of Elasticity (E) (GPa)	Modulus of Compressibility (K) (GPa)	Modulus of Elasticity in Shear (G) (GPa)	Vickers Hardness Number (H) (Kg/mm^2)
T1	0.526	0.236	70.23	44.35	28.41	655.91
T2	0.543	0.244	80.17	52.28	32.21	759.83
T3	0.585	0.262	94.48	66.27	37.42	923.63
T4	0.622	0.277	109.24	81.49	42.79	1096.97
T5	0.677	0.295	128.45	104.31	49.60	1338.51

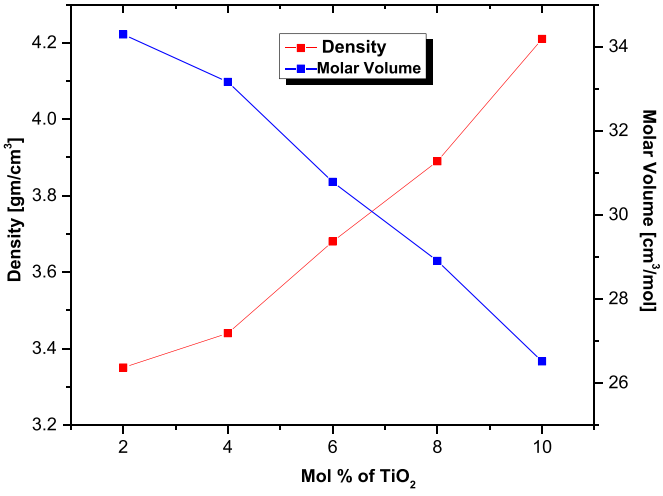

Fig. 7. Density and molar volume of TiO_2 doped glasses.

where V_i is packing factor of oxides, x_i is the mole fraction of oxides and V_m is the molar volume of the prepared glasses. V_i is calculated by using the equation given in [86–88].

APF of the system increases with an increase in a mole percent of titanium oxide (Table 4). The addition of TiO_2 modifies the glass network by enhancing the rigidity of glasses.

3.8. Elastic properties

The rigidity of glasses is also explained with the help of Poisson's ratio (σ) which can be calculated by using the equation [86–88].

$$\text{Poisson's ratio } (\sigma) = (0.5) - \left(\frac{1}{7.2V_T}\right)$$

Any change in the cross link density of glass network directly affects its value of Poisson's ratio. For three-dimensional glasses like silicon oxide glasses (SiO_2), the Poisson ratio has value 0.15, whereas for a two-dimensional structure like borate glasses (B_2O_3), it has a value approximately 0.3 [89–91].

The Poisson's ratio gets augmented continuously with the insertion of titanium in a given glasses system (Table 4) which enhanced the stiffness of the glasses by decreasing its dimensionality.

The elastic properties of the prepared glasses have been evaluated by using Yamane and Mackenzie's procedure [86,87].

The theoretical values of Young's modulus (E) are estimated from the values of V_T and dissociation energy with the help of standard relations adopted elsewhere [87]:

$$\text{Young's modulus } (E) = 83.6\, V_T \sum G_i x_i$$

Where G_i are the Dissociation energies per unit volume and x_i.

In glasses, both bulk modulus (K) and shear modulus (G) are known to be related to Young's modulus (E) and Poisson's ratio (σ) by the equations [87].

$$\text{Bulk modulus } (K) = \frac{E}{3(1-2\sigma)}$$

$$\text{Shear modulus } (G) = \frac{E}{2(1+2\sigma)}$$

The packing density V_i and the dissociation energy G_i obtained in the present study are listed. The glasses structure is well characterized by the results of Young's modulus, bulk modulus (K) and shear modulus (G) calculation. The value of these parameters is affected for any amendment in the temperament of the chemical bond and its strength in the glass matrix. These are especially valuable in exploring the alteration in the cross-link density of glasses. It has been observed in prepared glasses that the value of elastic moduli increased almost in linear manner with increasing the content of TiO_2. This indicates that titanium oxide addition helps to increase the glasses' rigidity due to change in the structural units BO_3 into tightly packed units BO_4. The higher value of the bulk modulus is confirmed by the increase in number of bonds (n_b) in a unit volume of glass and value of average coordination as given in Table 3. The variation of elastic constants with mol% of TiO_2 of glasses is shown in Fig. 8.

The Vickers hardness number of glass is calculated by the equation given by M. Yamane and J.D. Mackenzie [87]. It has been seen that hardness of the glasses gets enhanced with enhancement in the mol% of TiO_2 which once more supports the density, molar volume and band gap results.

3.9. Gamma ray shielding parameters

The theoretical values related with photon attenuation ability of the studied glasses are examined at a particular choice of energy with the help of Phy-X/PSD software [92]. It can exploit the numerous shielding parameters accurately at any energy range; like LAC (linear attenuation coefficient), half value layer (HVL), mean free path and Exposure Buildup (EBF) etc. [93].

3.9.1. Linear attenuation Coefficient (LAC) (μ)

LAC measurement is vital tool to find out the shielding ability of any material. The variation of LAC (μ) with the concentration of TiO_2 as a function of photon energies 0.015–15 MeV for the present glass samples is plotted in Fig. 9. It is clear that the LAC value increases from 197.756 to 221.523 cm^{-1} for the samples T1 to T5 indicating its compositional dependence with TiO_2. The values of LAC decreases sharply in low energy region (0.015–0.06 MeV) and gradually in intermediate energy range (0.06–1 MeV). This behaviour of LAC values is attributed to various possibilities of interaction of gamma rays with glasses. There are three main causes of the variation in LAC; first at low energy, where the photoelectric effect is a dominant mechanism; second at intermediate energy, where Compton scattering plays the role in declining the LAC values and third one

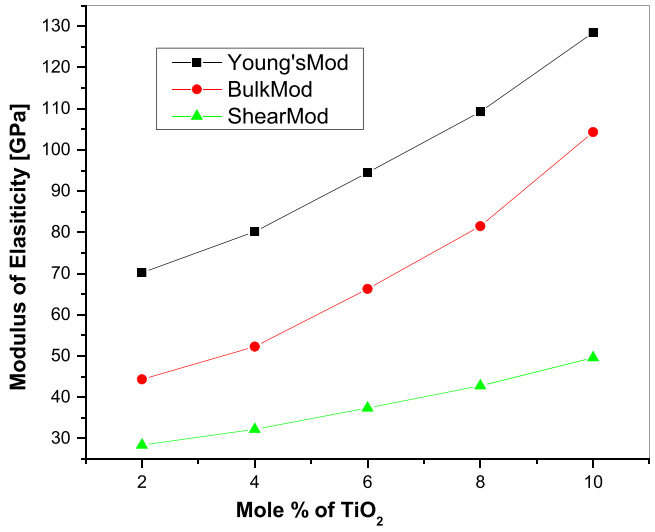

Fig. 8. Elastic constants variation with mol% of TiO_2 of Glasses.

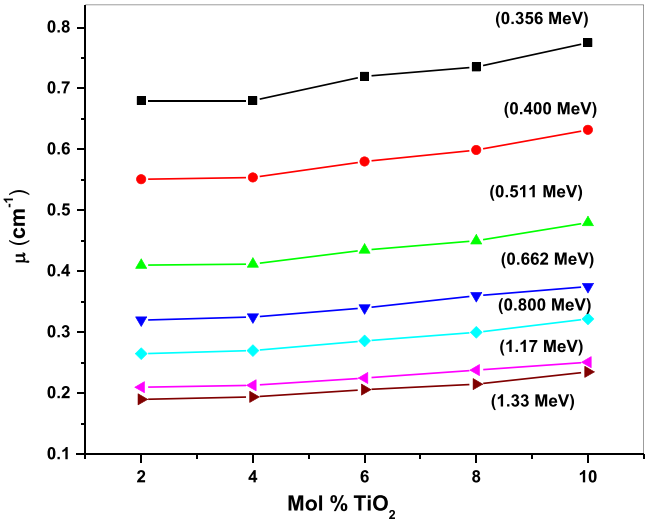

Fig. 10. Variation of Linear attenuation coefficient of glasses with mol% of TiO_2 at selected photon energy.

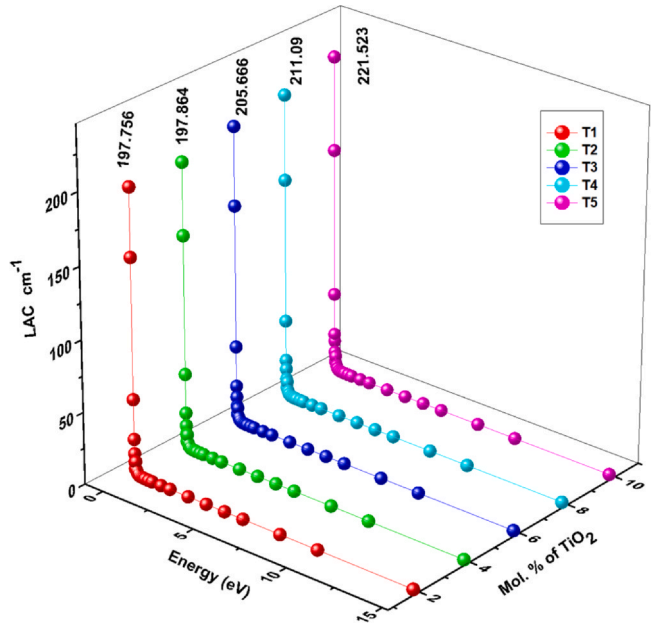

Fig. 9. Variation of Linear attenuation coefficient of glasses with mol% of TiO_2.

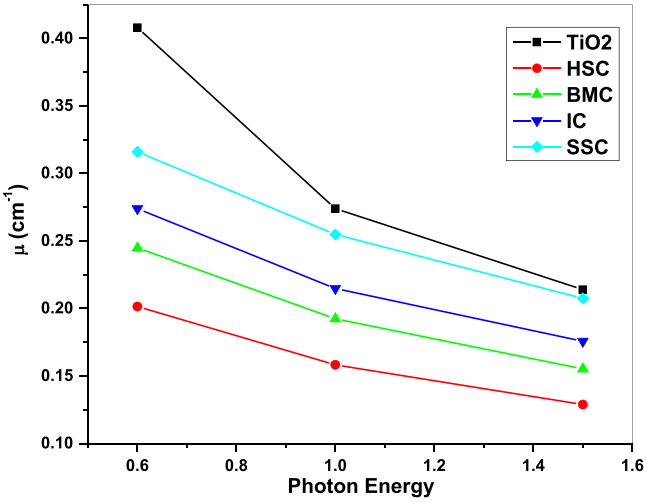

Fig. 11. Comparison of Linear attenuation coefficient with some concretes.

corresponds to pair production which occurs at photon energies higher than 1 MeV. The variation of LAC (μ) for present CB (Cerium Borate) glasses with mol% of TiO_2 at selected photon energies 0.356 MeV, 0.662 MeV, 1.17 MeV and 1.33 MeV is illustrated in Fig. 10. The observations mark that at each particular value of energy, μ of glass samples increases with the increase in concentration of TiO_2. These results are just similar to the results reported in different glass systems i.e μ depends on content of higher atomic weight oxide present in the glass network [93]. Fig. 10 also indicates that attenuation coefficient varies inversely to the photon energy (at higher photon energy μ has lower value). At 0.356 MeV energy, T5 glass has higher linear attenuation coefficient (0.775 cm^{-1}) but at 1.50 MeV energy, value of μ decreases continuously (0.235 cm^{-1}). It has also been noticed that μ decreases abruptly in the beginning with small increase in photon energy which is due to photoelectric effect, and this variation is smaller in the mid region of photon energy due to Compton scattering and almost constant at higher energy value more than 5 MeV. Since Hematite serpentine concrete (HSC), Basalt Magnetite concrete (BMC), Ilmenite Concrete (IC) and Steel Scrap concrete (SSC) are reported as best shielding materials [94], so to find out superlative attenuation capacity in prepared titanium glasses, we have compared the μ of T5 glass sample with above mentioned concretes at selective energy values 0.6, 1 and 1.5 MeV as shown in Fig. 11. It indicates that T5 glass has value higher than these concretes. So, it may be concluded that TiO_2 doped glasses help to improve attenuation ability of glasses towards gamma radiation.

3.9.2. Half value layer (HVL) and Mean free Path (MFP)

Phy-X/PSD program is utilized to acquire the HVL and MFP values which are very important parameters to find out gamma radiation blocking tendency of any materials. The material that has lesser value of these two parameters will have a better shielding proficiency. As depicted in Figs. 12 and 13, MFP and HVL values of these glasses got diminished with rise in photon energy and also with the concentration of TiO_2. The deviation of HVL with TiO_2 mol% at selected energy values 0.356, 0.662, 1.17 and 1.33 MeV are represented in Fig. 14 that signifies that as the contents of titanium increases, HVL decreases continuously at selected energy value. Also the HVL of these glasses compared with Ordinary Concrete, Barite, Ferrite, chromite, serpentite concretes and radiation shielding glasses

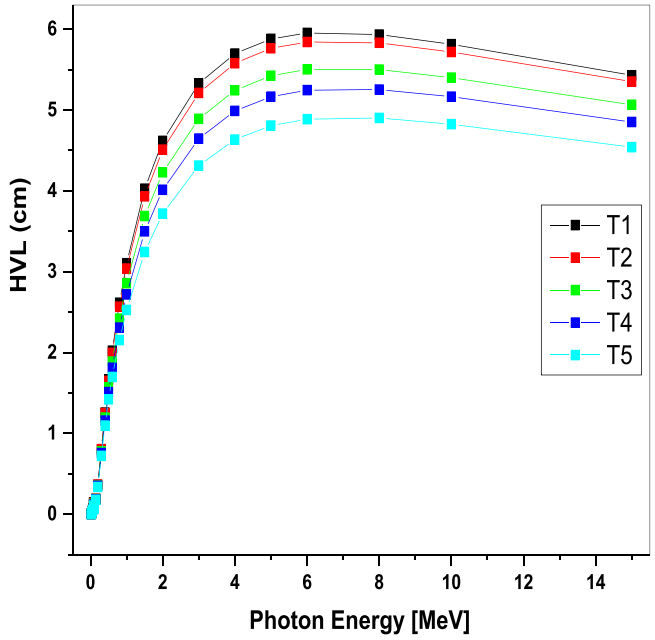

Fig. 12. Variation of HVL of glasses with photon energy.

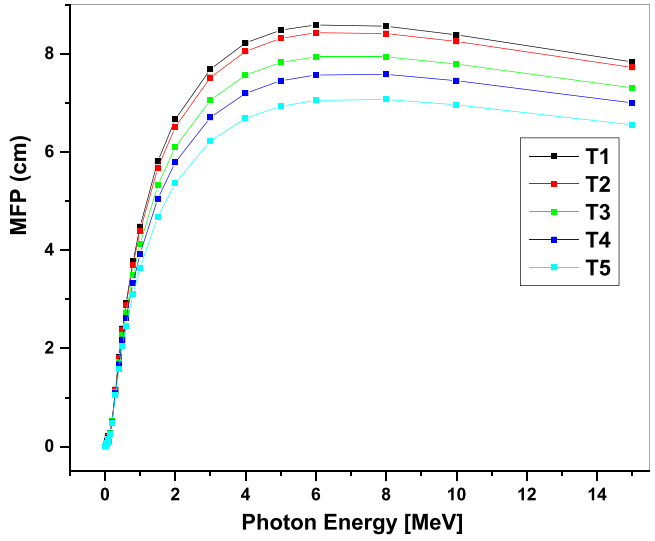

Fig. 13. Variation of MFP of glasses with photon energy.

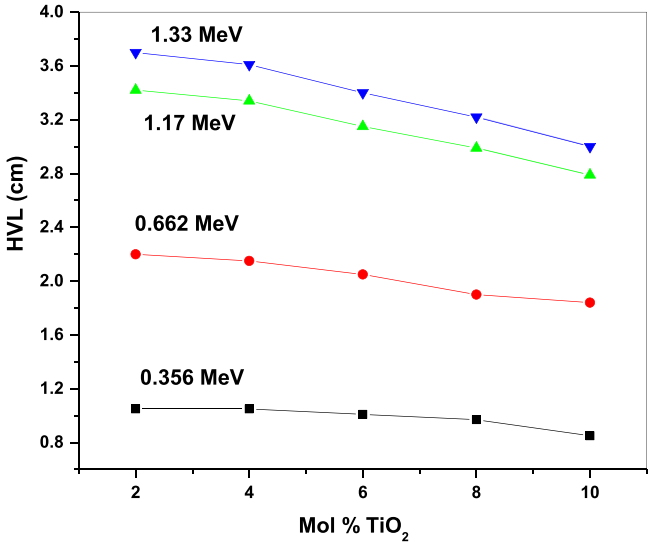

Fig. 14. Variation of HVL of glasses with mol% of TiO_2.

Table 5
Comparison of HVL of prepared glass samples with other radiation shielding concretes and glasses.

Glass	0.356 (MeV)	0.662 (MeV)	1.17 (MeV)	1.33 (MeV)
T1	1.05	2.2	3.42	3.7
T2	1.05	2.15	3.34	3.61
T3	1.01	2.05	3.15	3.4
T4	0.97	1.9	2.99	3.22
T5	0.85	1.84	2.79	3
Ordinary Concrete	2.96	3.87	5.09	5.43
Barite	2	2.54	3.5	3.75
Ferrite	1.5	1.98	2.62	2.79
Chromite	2.05	2.82	3.72	3.97
Serpentite	3.05	4.07	6	6.40
RS253G18	2.61	3.5	4.98	5.5
RS360	1	2.01	3.41	3.85

Rs253G18 and RS360 as shown in Table 5. This comparison shows that TiO_2 glasses have better shielding ability than concretes. It has been reported that the Hematite serpentine concrete (HSC), Basalt Magnetite concrete (BMC), Ilmenite Concrete (IC) and Steel Scrap concrete (SSC) are best shielding materials [94]. We have matched up to their MFP values with T5 sample (10% TiO_2) as exposed in Fig. 15. This helps to conclude that the MFP for the T5 sample has lower value than different concretes. We have also evaluated the MFP of T5 sample against the MFP value of some commercial glasses RS323G19, RS360 and RS520 made by Schott Company [95] shown in Fig. 16. This comparison is again in the support that T5 glass composition has better shielding ability as compared to RS323G19 and RS360 materials. Hence this composition of glasses (T5) can be build up as superior radiation safe guard material.

3.9.3. Exposure buildup and energy absorption buildup factors (EBF and EABF)

The photon energy and penetration depths (1–40 cm^{-1}) tend to change the EBF and EBAF values of titanium doped glasses as shown in Fig. 17 and Fig. 18 since in the phenomenon of photoelectric effect, the photons are totally absorbed, so minimum values of EBF and EABF of the glass samples are produced at low photon energy. As energy of the photon boosts at an intermediate energy region, this causes an increase in EBF and EABF values of glasses and this behaviour may be attributed to Compton Effect's multiple scattering. At higher energy, the values of EBF and EABF show an increment which may possibly be a result of pair production [6,97]. The pair

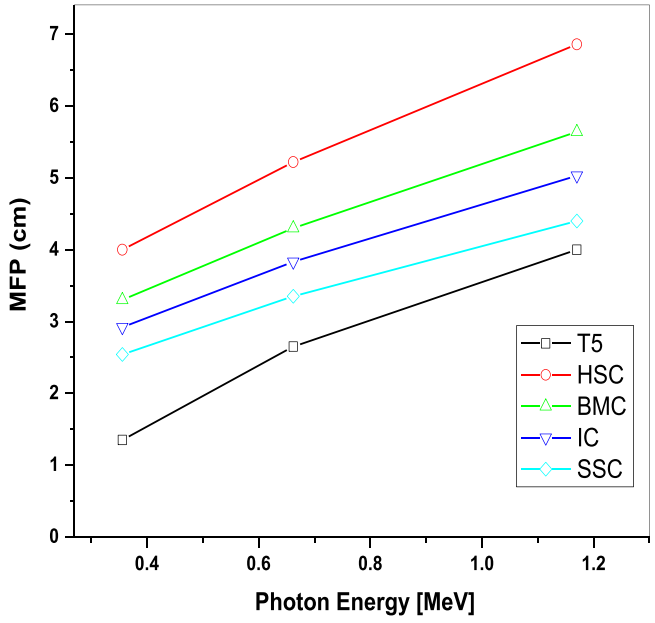

Fig. 15. Comparison of MFP with some concretes.

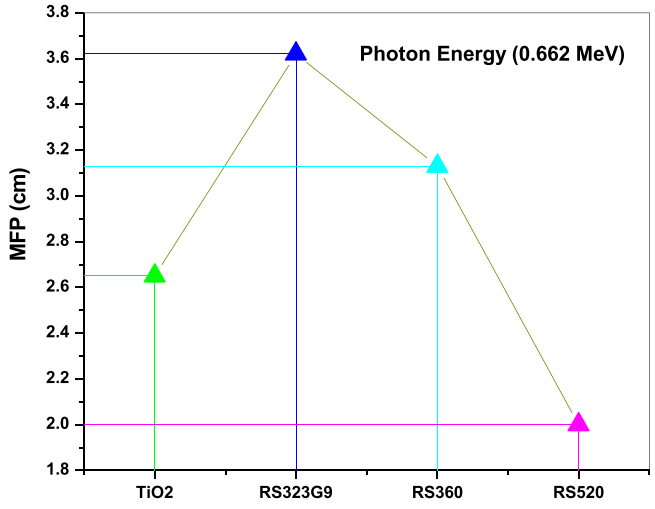

Fig. 16. Comparison of MFP with some commercial glasses.

production cross-section gets altered with equivalent atomic number as $(Z_{eq})^2$. So, a higher probability of pair-production is experienced by the glass having higher $Z_{eq.}$ [96,97]. The investigation illustrates that the sample T5 with high concentration of titanium has lowest value of EBF and should be considered for gamma-ray shielding.

The variation of EBFs of the glasses with penetration depths at particular photon energies is depicted in Fig. 19. The EBF values show an increasing trend with the enhancement in penetration depths since at high penetration depths, many more scattering events occur and it happens at particular value of incident energy (1, 3, 5, 10 and 15 MeV) [96]. It is noticed that values of EBF increases with rise in mfp. The buildup factors are quickly developed at higher penetration depths (20–40 mfp) as the pair production cross-section changes to Z^2 at high energies [6]. At 1 MeV energy sample T5 has highest value of EBF. But at 3 MeV, values of EBF are almost not dependent on chemical composition of glasses and there is nearly a constant magnitude of EBF. The reason behind this may be the compton scattering as it is the main interacting process in this region for glasses whose cross-section varies linearly with Z_{eq} [97]. Consequently, there is not any remarkable variation of EBF at this energy. At energy more than 3 MeV, the trend of EBF values gets reversed. The same trend has been observed by many researchers in their studies [97–101]. The reason for this trend may be the dominance of the phenomenon of pair production in this energy region. Here, EBF decreases with increase in molar concentration of titanium oxide as is evident from Fig. 19. The EBF value is less for T5 sample in the energy range 3–15 MeV which contains high concentration of TiO_2. This is a known fact that the material with low EBF and high effective atomic number is a good shielding material. Hence it is revealed that high titanium concentration makes the glass sample a better radiation shielder in terms of buildup factor [98–101].

Dependence of EBFs on the atomic number of elements indicates that the value of EBF of the materials is also dependent on its chemical compositions [100,101]. EBF dependency on chemical composition is analyzed with energy at constant penetration depths shown in Fig. 20. It is observed that the EBF values are small at low energy photons whereas maximum at higher energy photons. The reason behind this variation is the photo-electric and pair-production which are dominant interaction processes in low- and high-energy, respectively that completely removes the photons. The sample T5 has lower EBF value as compared with other glass samples. These results indicate that higher concentration of titanium in glasses is favourable to enhance the shielding efficiency towards the gamma radiations.

The EBF values of T5 glasses and some concretes of steel-magnetite (SM), Ilmenite-limonite (IL), Ordinary Concrete (OC), Steel-scrap (SC) and Lead have been compared and are given in Table 6 [99]. The buildup factors of TiO_2 glasses are found to be lesser than all concretes which indicate that titanium glasses are appropriate for producing some shielding materials [96].

3.9.4. Neutron attenuation

The fast neutron removal cross section (FNRCS in cm^{-1}) ($\sum_R$) plays an important role to check the ability of the medium to block the neutron beam in fast (or fission energy) neutron attenuation. FNRCS helps to measure the probability for the happening of first interaction that removes the incident neutron. The fast neutron removal cross section (FNRCS) for the mentioned glasses has been calculated by using the equation mentioned elsewhere [92]. It is observed that $\sum_R$ value enhances with titanium concentration in the glass matrix that may be because of increasing density of glass samples with rise in titanium contents. The FNRCS value of the glasses prepared in this study and some other neutron shielding concretes/glasses (SBC-B35 glass, Graphite, HSC, ILC, Ordinary concrete and Basalt magnetite concrete (BMC) has been compared as depicted in Fig. 21 [96,100–102]. It is found that neutron shielding capability of glasses prepared in this study is more than previously stated glasses/concretes. The prepared glasses prove to be very effective in attenuating the fast neutrons as inferred from the comparison of $\sum_R$ values of studied glasses to that of water which is considered as a good neutron absorber (0.1023 cm^{-1}) [96]. Table 7 revealed that FNRCS of T5 glass has higher value than many good neutron shielding glasses studied by different researchers [103–106].

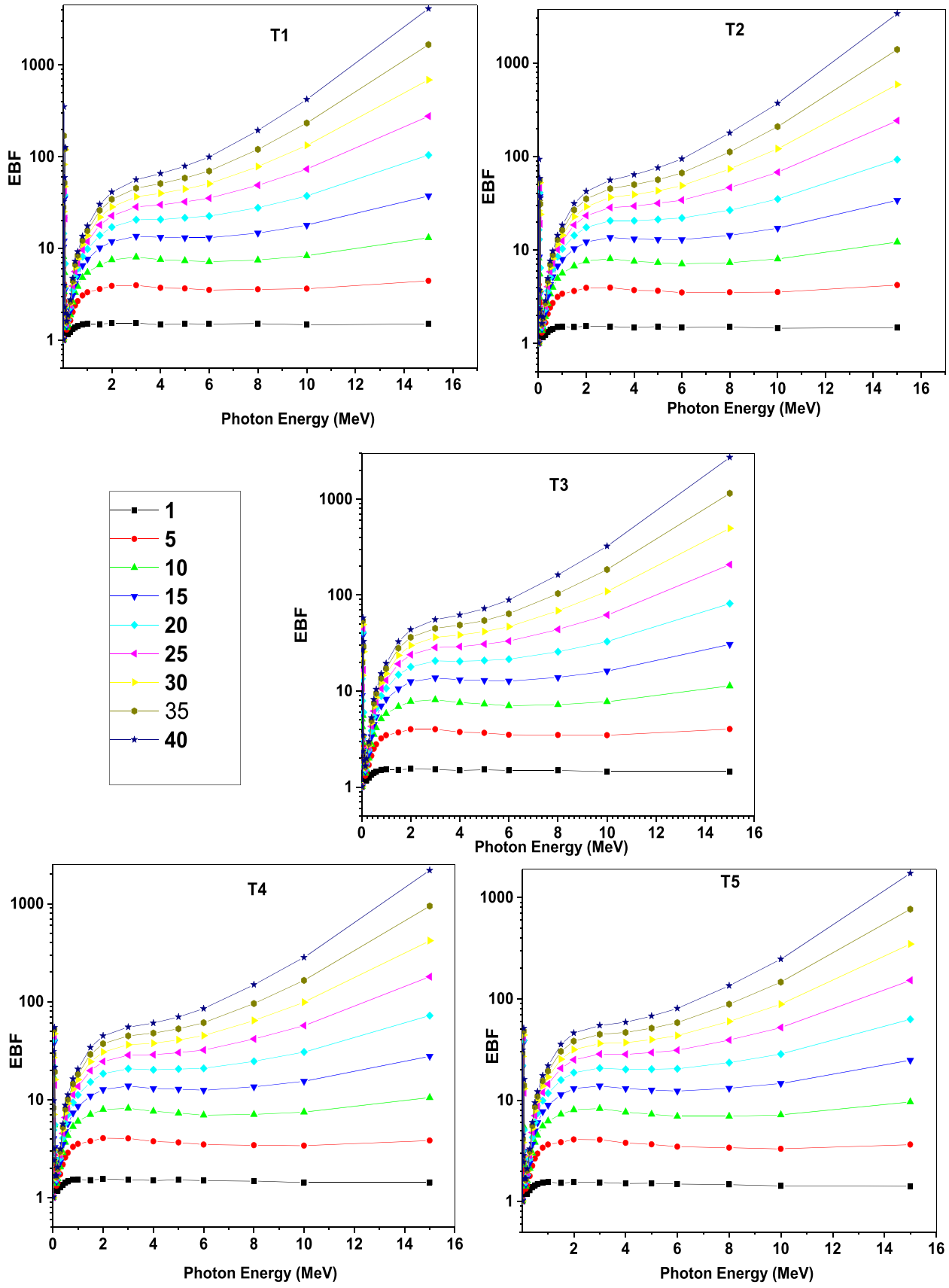

Fig. 17. Variation of EBF with photon energy.

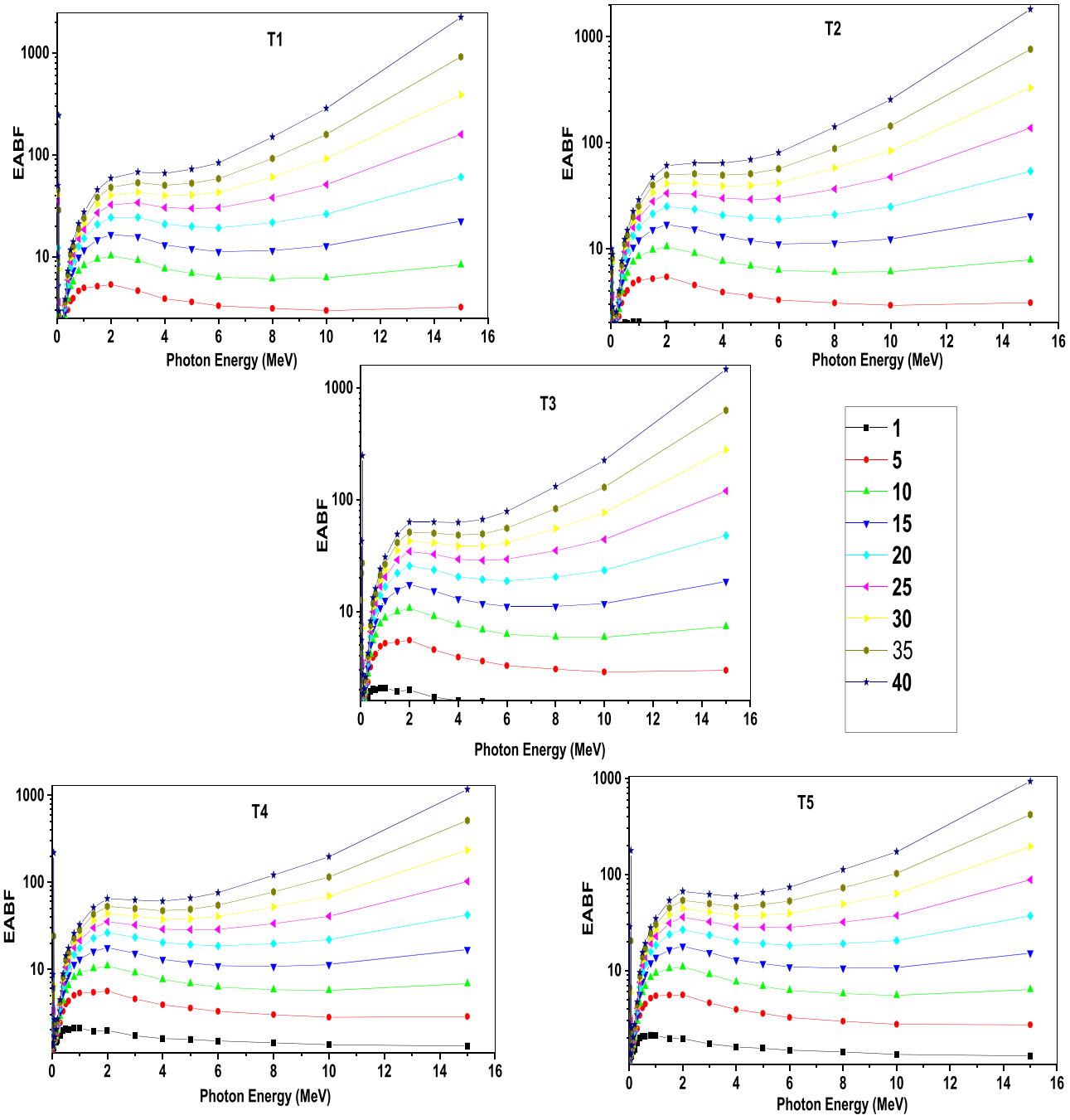

Fig. 18. Variation of EABF with photon energy.

For thermal neutrons, boron is a well-known candidate for its outstanding shielding property [96]. So the presence of boron has a remarkable impact in improving the neutron absorbing/attenuating properties of the mentioned glasses. The total cross-section (σ_T) gives the probability when a neutron interacts with the target nuclei, whatever may be the interaction type. In present study, the total cross-section (σ_T) to find the neutron attenuation is expressed by the relation [97], $(\sigma_T)=(\sigma_c)+(\sigma_{ic})+(\sigma_A)$ Where σ_c is the coherent and σ_{ic} is the incoherent scattering cross-section and σ_A denotes the absorption cross-section due to nuclear capture processes. The values σ_c, σ_{ic}, σ_A, and σ_T calculated by using the given formula reported in [96,107,108] for all samples is shown in Table 8 and it can be found that all these values increase with increase in TiO_2 contents. Moreover, the T5 sample has highest σ_T and Σ_T value among all the glass samples. Thus, comparing the titanium element content of all glasses, we can conclude that more the titanium content in samples, better be the thermal neutron shielding features. So T5 glass sample is preferred for thermal and fast neutron attenuation.

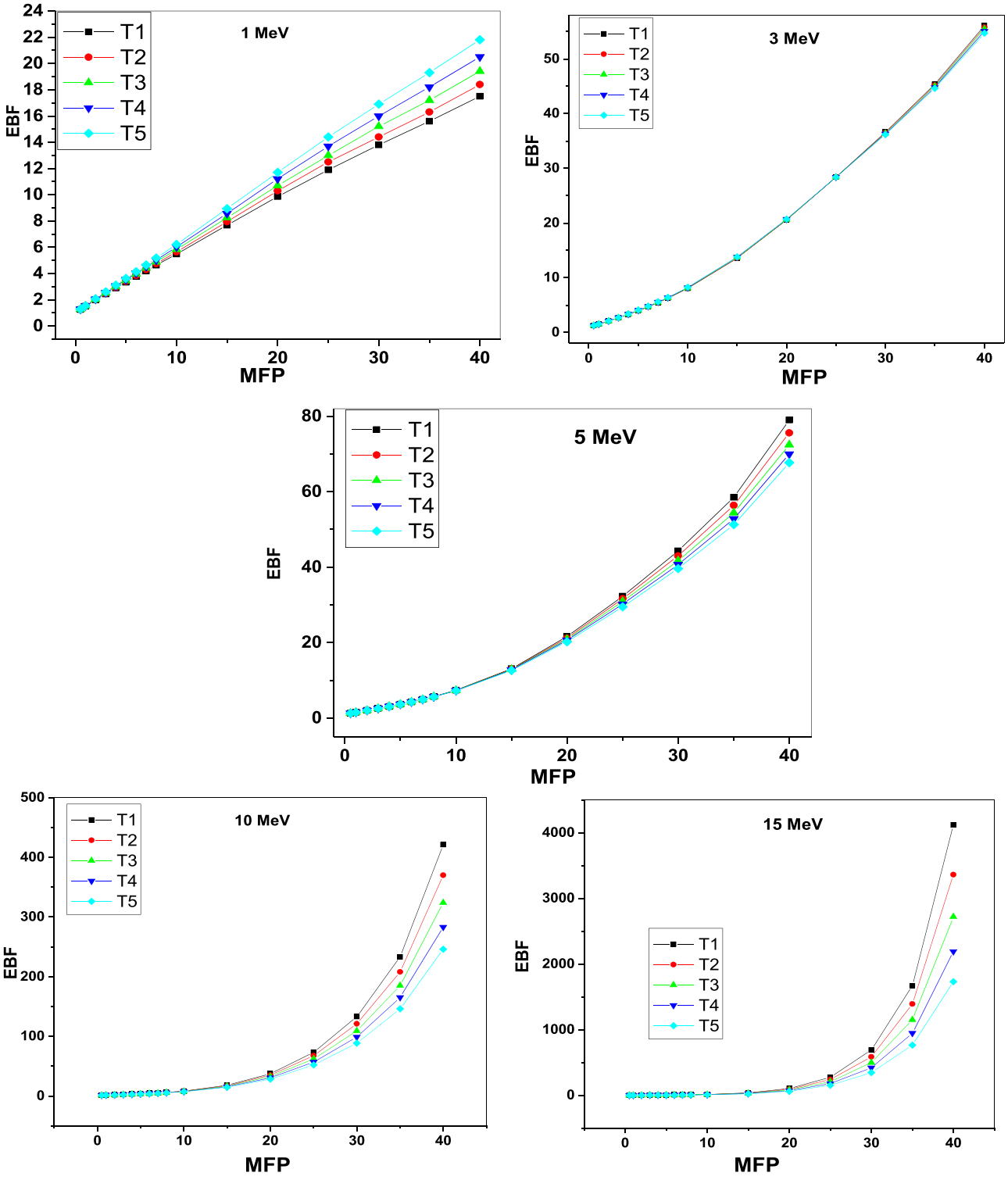

Fig. 19. Variation of EBF with MFP at particular photon energy.

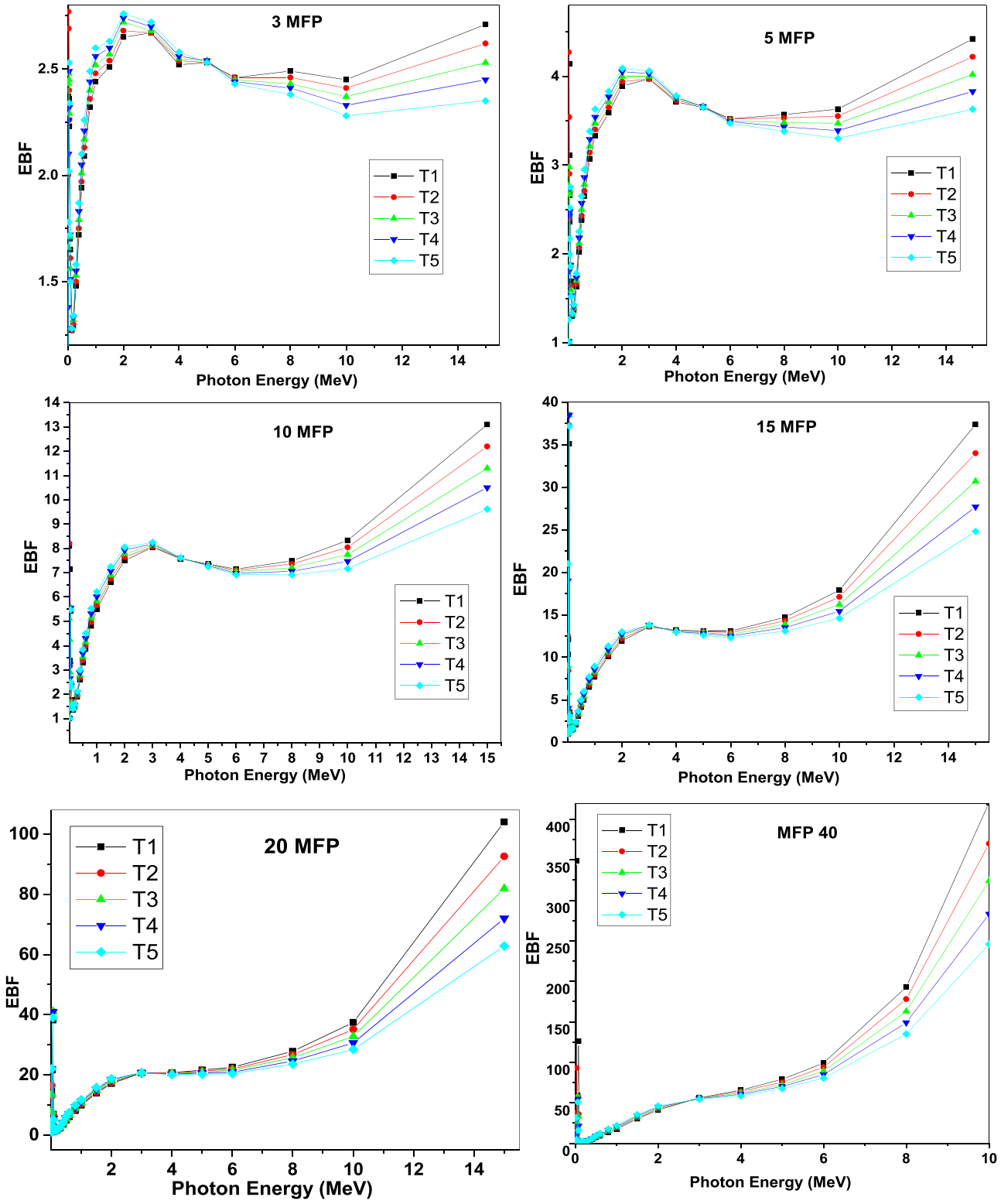

Fig. 20. Variation of EBF with photon energy at different MFP.

Table 6
Comparison of EBF of T5 glasses with Ordinary Concrete(OC), Ilmenite-limonite (IL), Steel-scrap (SC), steel–magnetite (SM) and Lead.

0.15 MeV						
MFP	**T5**	**OC**	**IL**	**SC**	**SM**	**Lead**
1	1.19	2.91	1.99	1.87	1.79	1.4
5	1.33	16.68	5.59	1.96	4.19	1.84
10	1.41	50.1	10.23	1.96	6.83	2.13
20	1.55	193.53	21.19	1.96	12.34	2.87
40	1.68	940.68	46.1	1.94	22.89	6.65
1.5 MeV						
MFP	**T5**	**OC**	**IL**	**SC**	**SM**	**Lead**
1	1.52	1.91	1.8	1.78	1.76	1.38
5	3.83	7.19	6.17	6.07	5.87	2.74
10	7.25	16.42	13.46	13.37	12.75	4.47
20	15.8	40.34	31.89	32.65	30.45	8.11
40	35.48	105.85	77.84	85.17	76.26	15

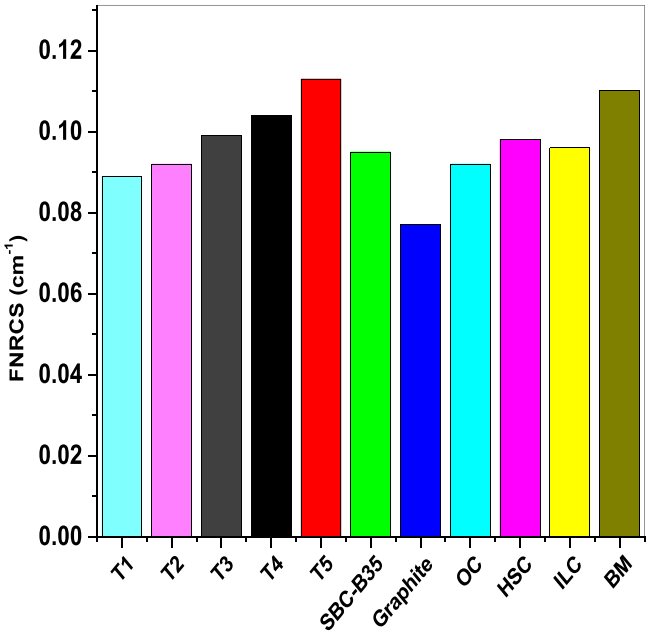

Fig. 21. Comparison of fast neutron removal cross section with some commercial glasses/concretes.

Table 7
Comparison of FNRCS of T5 glasses with other shielding glasses.

Glass	**FNRCS (cm^{-1})**
T5	0.113
TVM60	0.106
VPZn8	0.092
S2 Ceramics	0.070
C20 glass	0.107

Table 8
Coherent scattering cross-section (σc), absorption cross-section (σ_A), incoherent scattering cross-section (σ_{ic}), total cross-section (σ_T) and macro cross section (Σ_T) of glasses for thermal neutron attenuation.

Glass	σ_c	σ_A	σ_{ic}	σ_T	Σ_T
T1	0.306	18.322	0.054	18.682	3.28134
T2	0.309	18.394	0.059	18.762	3.40815
T3	0.324	19.221	0.067	19.612	3.8386
T4	0.335	19.829	0.075	20.239	4.21779
T5	0.355	20.924	0.085	21.364	4.85376

4. Conclusion

The reported work presents the additive impact of TiO_2 on the physical, elastic and optical properties of cerium based borate glasses. The recent investigation also aimed to study comprehensively that the radiation shielding properties of studied glasses varied with composition. Accordingly, Phy-X/PSD software was utilized to estimate LAC (Linear Attenuation Coefficient), HVL (Half Value Layer), MFP (Mean Free Path) values including Exposure Buildup and Energy Absorption Buildup factors of these glasses. To further facilitate the shielding design, estimation of the fast and thermal neutron removal cross section has been done. The results derived henceforth are summed up below:

1. The absence of sharp peaks in XRD pattern confirms the amorphous nature of all glass samples.
2. Optical spectral studies indicated that a strong UV-shielding effect is observed in T3-T5 samples. In addition, a band is observed in the optical absorption spectra at about 480 nm and grows in the glass samples T4-T5 having high concentration of TiO_2. This indicates the increase in number of Ti^{3+} ions at the expense of reduction of Ti^{4+} ions. The glasses showed a strong UV-blocking efficiency also as they blocked all the three regions of UV (UVA, UVB and UVC) making them suitable to be used as transparent UV shielding materials or UV filters. Lower values of band gap energy (2.25–2 eV) indicate higher degrees of disorder in these glasses. The refractive index increases from 2.64 to 2.74 which is possibly due to replacement of borate oxide by high atomic mass and high field strength TiO_2.
3. FTIR spectroscopy revealed that glass structure is primarily composed of BO_3 and BO_4 structural units. As TiO_2 concentrations are made higher, there is observation of Ti^{3+} and Ti^{4+} ions in glass samples and a structural modification appears because there is development of TiO_4 and TiO_6 groups.
4. Outcome of physical (molar volume, density) and elastic parameters (Young's modulus, shear modulus and Vickers number) exposed that the glasses' stability gets augmented by adding TiO_2 content. As TiO_2 increases, correspondingly theoretical optical basicity and electronic polarizability of glasses also increase. The TPA of glasses increases gradually from 18.54 to 20.56 with the inclusion of titanium oxide which indicates that these glasses may be useful in some photonic devices.
5. The studies carried out on radiation interaction parameters and attenuation properties of prepared glass samples depict that T5 glass sample is set up to have superior gamma-ray shielding efficiency owing to its elevated linear attenuation μ and declined MFP values. Additionally, this sample T5 has poorer HVLs than those of other concretes and commercial glass samples apart from RS520 commercial glass. Finally, after comparing our results with some gamma shielding glasses reported in the past, we can conclude that by adding TiO_2, attenuation performance of investigated glasses is improved. The glass which has high concentration of titanium (T5 sample) has lower value of EBF as compared to OC, IL, SMC concretes.
6. Thermal and fast neutron shielding results showed that the neutron attenuation ability has higher value for T5 glass which has higher concentration of TiO_2.

In Conclusion, researchers have always been motivated to discover superior, new-generation and eco-friendly shielding materials since radiations have found their use extensively in different fields such as medicine or health services, agriculture, nuclear power industry, exploration of space etc. The recent work is one such initiative to find modification of a base borate glass system on adding TiO_2 such that it may be used in radiative environments and also to have an insight in structure of these glasses.

CRediT authorship contribution statement

Gurinder Pal Singh: Conceptualization, Methodology, Investigation, Resources, Writing - original draft preparation, Validation, Visualization, Software, Writing - review & editing, Data Curation, Supervision. **Joga Singh:** Writing - review & editing, Validation. **Parvinder Kaur:** Writing - review & editing, Validation. **Taminder Singh:** Validation. **Simranpreet Kaur:** Validation. **Ravneet Kaur:** Writing - review & editing, Validation. **D.P. Singh**: Resources, Methodology, Visualization, Validation, Supervision.

Declaration of Competing Interest

The authors declare that they have no known competing financial interests or personal relationships that could have appeared to influence the work reported in this paper.

References

[1] J. Valentin, The 2007 recommendations of the international commission on radiological protection, Elsevier, 2008, pp. 1533–1544.
[2] K.E. Thomas, J.E. Parnell-Parmley, S. Haidar, R. Moineddin, E. Charkot, G. BenDavid, C. Krajewski, Assessment of radiation dose awareness among pediatricians, Pediatr. Radiol. 36 (8) (2006) 823–832.
[3] M.S. Al-Buriahi, Y.S.M. Alajerami, A.S. Abouhaswa, Amani Alalawi, Tanin Nutaro, Baris Tonguc, Effect of chromium oxide on the physical, optical, and radiation shielding properties of lead sodium borate glasses, J. Non Cryst. Solids 544 (2020) 120171.
[4] Adem Un, F. Demir, Determination of mass attenuation coefficients, effective atomic numbers and effective electron numbers for heavy-weight and normal-weight concretes, Appl. Radiat. Isot. 80 (2013) 73–77.
[5] O. Agar, H.O. Tekin, M.I. Sayyed, Mehmet E. Korkmaz, Ozgur Culfa, C. Ertugay, Experimental investigation of photon attenuation behaviors for concretes including natural perlite mineral, Results Phys. 12 (2019) 237–243.
[6] Gokhan Kilic, Shams A.M. Issa, Erkan Ilik, O. Kilicoglu, H.O. Tekin, A journey for exploration of Eu_2O_3 reinforcement effect on zinc-borate glasses: synthesis, optical, physical and nuclear radiation shielding properties, Ceram. Int. 47 (2) (2021) 2572–2583.
[7] S.S. Obaid, D.K. Gaikwad, P.P. Pawar, Determination of gamma ray shielding parameters of rocks and concrete, Radiat. Phys. Chem. 144 (2018) 356–360.
[8] S.S. Obaid, M.I. Sayyed, D.K. Gaikwad, H.O. Tekin, Y. Elmahroug, P.P. Pawar, Photon attenuation coefficients of different rock samples using MCNPX, Geant4 simulation codes and experimental results: a comparison study, Radiat. Eff. Defects Solids 173 (2018) 900–914.
[9] Ozge Kilicoglu, H.O. Tekin, Bioactive glasses with TiO_2 additive: Behavior characterization against nuclear radiation and determination of buildup factors, Ceram. Int. 46 (8) (2020) 10779–10787.
[10] Z. Xie, Q. Du, Y. Wu, X. Hao, C. Liu, Full-band UV shielding and highly daylight luminescent silane-functionalized graphene quantum dot nanofluids and their arbitrary polymerized hybrid gel glasses, J. Mater. Chem. C 4 (2016) 9879–9886.
[11] M. Eita, L. Wagberg, M. Muhammed, Spin-assisted multilayers of poly(methyl methacrylate) and zinc oxide quantum dots for ultraviolet-blocking applications, ACS Appl. Mater. Interfaces 4 (2012) 2920–2925.
[12] F. Akman, M.I. Sayyed, M.R. Kaçal, H.O. Tekin, Investigation of photon shielding performances of some selected alloys by experimental data, theoretical and MCNPX code in the energy range of 81 keV–1333 keV, J. Alloys Compd. 772 (2019) 516–524.
[13] W. Chen, J. Hong, H. Li, Y. Li, Fabrication and ultraviolet-shielding properties of silica-coated titania-doped ceria nanoparticles, J. Rare Earths 29 (2011) 810–814.
[14] Yuncheng Jiang, Luping Wang, Wenna Zhang, Liming Teng, Fangfang Hu, Hai Guo, Dual-valence Ce doped UV-shielding glasses with high transparency and stability, Ceram. Int. 46 (2020) 16032–16037.
[15] Pichitchai Butnoi, Narong Chanlek, Yingyot Poo-arporn, Supree Pinitsoontorn, Santi Maensiri, Pinit Kidkhunthod, Structure-function of novel glasses for possibility as cathode of Li-ion battery: lithium manganese borate glasses, J. Alloys Compd. 809 (2019) 151811.
[16] S.A.M. Abdel-Hameed, A.M. Fathi, M. Eltohamy, Structure, optical and electrical behaviour of $x(2Bi_2O_3.MnO).(10-x)B_2O_3$ glasses, J. Non Cryst. Solids 510 (2019) 71–80.
[17] A. El-Denglawey, Hesham M.H. Zakaly, K. Alshammari, Shams A.M. Issa, H.O. Tekin, Waheed S. AbuShanab, Yasser B. Saddeek, Prediction of mechanical and radiation parameters of glasses with high Bi2O3 concentration, Results Phys. 21 (2021) 103839.
[18] D. Moncke, E.I. Kamitsos, D. Palles, R. Limbach, A. Winterstein-Beckmann, T. Honma, Z. Yao, T. Rouxel, L. Wondraczek, Transition and post-transition metal ions in borate glasses: borate ligand speciation, cluster formation, and their effect on glass transition and mechanical properties, J. Chem. Phys. 145 (12) (2016) 124501.
[19] A. Herrmann, H.A. Othman, A.A. Assadi, M. Tiegel, S. Kuhn, C. Rüssel, Spectroscopic properties of cerium-doped aluminosilicate glasses, Opt. Mater. Express 5 (2015) 720–732.
[20] D. Moncke, G. Tricot, A. Winterstein Beckmann, L. Wondraczek, E.I. Kamitsos, On the connectivity of borate tetrahedra in borate and borosilicate glasses, Phys. Chem. Glass 56 (5) (2015) 203–211.
[21] H. Masai, T. Yanagida, Emission property of Ce^{3+}-doped $Li_2O–B_2O_3–SiO_2$ glasses, Opt. Mater. Express 5 (2015) 1851–1858.
[22] Gokhan Kilic, Erkan Ilik, Shams A.M. Issa, H.O. Tekin, Synthesis and structural, optical, physical properties of Gadolinium (III) oxide reinforced TeO2–B2O3–(20-x)Li2O-xGd2O3 glass system, J. Alloys Compd. 877 (2021) 160302.
[23] H.O. Tekin, O. Kilicoglu, The influence of gallium (Ga) additive on nuclear radiation shielding effectiveness of Pd/Mn binary alloys, J. Alloys Compd. 815 (2020) 152484.
[24] A.S. Abouhaswa, Hesham M.H. Zakaly, Shams A.M. Issa, M. Rashad, Maria Pyshkina, H.O. Tekin, R. El-Mallawany, Mostafa Y.A. Mostafa, Synthesis, physical, optical, mechanical, and radiation attenuation properties of $TiO_2–Na_2O–Bi_2O_3–B_2O_3$ glasses, Ceram. Int. 47 (2021) 185–204.
[25] S. Kaur, G. Pal Singh, P. Kaur, D.P. Singh, Cerium luminescence in borate glass and effect of aluminium on blue green emission of cerium ions, J. Lumin. 143 (2013) 31–37.
[26] H.A. Othman, H.S. Elkholy, I.Z. Hager, FTIR of binary lead borate glass: structural investigation, J. Mol. Struct. 106 (2016) 286–290.
[27] Liwan Liu, Chongyun Shao, Yu Zhang, Xili Liao, Qiuhong Yang, Lili Hu, Danping Chen, Scintillation properties and X-ray irradiation hardness of Ce^{3+}-doped Gd_2O_3-based scintillation glass, J. Lumin. 176 (2016) 1–5.
[28] M.H.M. Zaid, K.A. Matori, H.A.A. Sidek, I.R. Ibrahim, "Bismuth modified gamma radiation shielding properties of titanium vanadium sodium tellurite glasses as a potent transparent radiation-resistant glass applications, Nucl. Eng. Technol. 53 (2021) 1323–1330.
[29] E.M. Abou Hussein, A.M. Madbouly, F.M. Ezz Eldin, N.A. ElAlaily, "Evaluation of physical and radiation shielding properties of Bi2O3–B2O3 glass doped transition metals ions, Mater. Chem. Phys. 261 (2021) 124212.
[30] Y.S. Rammah, M.S. Al-Buriahi, A.S. Abouhaswa, $B_2O_3–BaCO_3–Li_2O_3$ glass system doped with Co_3O_4: structure, optical, and radiation shielding properties, Phys. B Condens. Matter 576 (2020) 411717.
[31] Y. Ishii, K. Arai, H. Namikawa, M. Tanaka, A. Negishi, T. Handa, Preparation of cerium-activated silica glasses: phosphorus and aluminum codoping effects on absorption and fluorescence properties, J. Am. Ceram. Soc. 70 (2) (1987) 72–77.
[32] N. Chiodini, M. Fasoli, M. Martini, E. Rosetta, G. Spinolo, A. Vedda, M. Nikl, N. Solovieva, A. Baraldi, R. Capelletti, High-efficiency SiO_2:Ce^{3+} glass scintillators, Appl. Phys. Lett. 81 (23) (2002) 4374–4376.
[33] M.C. Rao, G. Ravi, Kumar, Influence of TiO_2 on structural, luminescent and conductivity investigations of $CaF_2–CaO–Y_2O_3–B_2O_3–P_2O_5$ glasses, Optik 179 (2019) 1109–1117.
[34] H. Singh, K. Singh, Leif Gerward, Kanwarjit Singh, H Singh Sahota, R Nathuram, ZnO–PbO–B_2O_3 glasses as gamma-ray shielding materials, Nucl. Instrum. Methods Phys. Res. Sect. B Beam Interact. Mater. At. 207 (2003) 257–262.
[35] H.A. Saudi, W.M. Abd-Allah, Structural, physical and radiation attenuation properties of tungsten doped zinc borate glasses, J. Alloys Compd. 860 (2021) 158225.
[36] A. Temir, K.S. Zhumadilov, M.V. Zdorovets, A. Kozlovskiy, A.V. Trukhanov, Study of the effect of doping CeO_2 in TeO2–MoO–Bi2O3 ceramics on the phase composition, optical properties and shielding efficiency of gamma radiation, Opt. Mater. 115 (2021) 111037.
[37] T. Alharbi, Hamdy F.M. Mohamed, Yasser B. Saddeek, Ahmed Y. El-Haseib, Kh.S. Shaaban, Study of the TiO_2 effect on the heavy metals oxides borosilicate glasses structure using gamma-ray spectroscopy and positron annihilation technique, Radiat. Phys. Chem. 164 (2019) 108345.
[38] B.P. Antonyuk, N.N. Novikova, N.V. Didenko, O.A. Aktsipetrov, All optical poling and second harmonic generation in glasses: theory and experiment, Phys. Lett. A 287 (2001) 161–168.
[39] B. Nagamani, Ch Srinivasu, Physical parameters and structural analysis of titanium doped binary boro silicate glasses by spectroscopic techniques, Mater. Today Proc. 18 (2019) 2077–2083.
[40] T. Satyanarayana, I.V. Kityk, K. Ozga, M. Piasecki, P. Bragiel, M.G. Brik, V. Ravi Kumar, A.H. Reshak, N. Veeraiah, Role of titanium valence states in optical and electronic features of PbO–Sb2O3–B2O3:TiO2 glass alloys, J. Alloys Compd. (2009) 283–297.
[41] R. Balaji Rao, G. Naga Raju, N. Veeraiah, Catalyzed crystallization and some physical properties of Li2O–MgO–B2O3:TiO2 glasses, Indian, J. Pure Appl. Mater. 43 (2005) 192–202.
[42] L. Koudelka, P. Mosner, M. Zeyer, C. Jager, Lead boro phosphate glasses doped with titanium dioxide, J. Non Cryst. Solids 326 (2003) 72–76.
[43] R. Balaji, A. Rosario, N. Veeraiah, Spectroscopic characterization, conductivity and relaxation anomalies in the $Li_2O–MgO–B_2O_3$ glass system: effect of nickel ions, J. Phys. Chem. 69 (2008) 2813–2826.
[44] H. Doweidar, K. El-Egili, R. Ramadan, M. Al-Zaibani, Structural units distribution, phase separation and properties of $PbO–TiO_2–B_2O_3$ glasses, J. Non Cryst. Solids 466–467 (2017) 37–44.
[45] K. Inoue, S. Sakida, T. Nanba, Y. Miura, Structure and optical properties of TiO_2 containing oxide glasses, Mater. Sci. Technol. Assoc. Iron Steel Technol. 3 (2006) 583–593.

[46] Liming Teng, Yuncheng Jiang, Wenna Zhang, Rongfei Wei, Hai Guo, Highly transparent cerium doped glasses with full-band UV-shielding capacity, J. Am. Ceram. Soc. 103 (2020) 3249–3256.

[47] A.M.B. Silva, R.N. Correia, J.M.M. Oliveira, M.H.V. Fernandes, Structural characterization of TiO_2–P_2O_5–CaO glasses by spectroscopy, J. Eur. Ceram. Soc. 30 (2010) 1253–1258.

[48] G. Naga Raju, Y. Gandhi, N. Srinivasa Rao, N. Veeraiah, Study on the influence of TiO_2 on the insulating strength of ZnO–ZnF2–B2O3 glasses by means of dielectric properties, Solid State Commun. 139 (2006) 64–69.

[49] R. Balaji Rao, D. Krishna Rao, N. Veeraiah, The role of titanium ions on structural, dielectric and optical properties of Li_2O–MgO–B_2O_3 glass system, Mater. Chem. Phys. 87 (2004) 357–369.

[50] R.M. Gunji, G.R.S. Mattos, C.D.S. Bordon, L.A. Gomez-Malagon, L.R.P. Kassab, Efficiency enhancement of silicon solar cells covered by GeO2–PbO glasses doped with Eu^{3+} and TiO_2 nanoparticles, J. Lumin. 223 (2020) 117244.

[51] Omar Romina Shafaghia, Sunjeev Rodriguez, Emil H. Phull, Paul Schemitsch, Stephen D. Zalzal, Marcello Waldman, Papini, R. Towler Mark, Effect of TiO2 doping on degradation rate, microstructure and strength of borate bioactive glass scaffolds, Mater. Sci. Eng. C 107 (2020) 110351.

[52] T.S. Bramhankar, S.S. Pawar, J.S. Shaikh, V.C. Gunge, N.I. Beedri, P.K. Baviskar, H.M. Pathan, P.S. Patil, R.C. Kambale, R.S. Pawar, Effect of Nickel–Zinc Co-doped TiO2 blocking layer on performance of DSSCs, J. Alloys Compd. 817 (2020) 152810.

[53] Taha Vosoughi Torbati, Vahid Javanbakht, Fabrication of TiO2/Zn2TiO4/Ag nanocomposite for synergic effects of UV radiation protection and antibacterial activity in sunscreen, Colloids Surf. B Biointerfaces 187 (2020) 110652.

[54] E.M. Abou Hussein, M.A. Maksoud, R.A. Fahim, A.S. Awed, Unveiling the gamma irradiation effects on linear and nonlinear optical properties of CeO_2–Na_2O–SrO–B_2O_3 glass, Opt. Mater. 114 (2021) 111007.

[55] Melis Gökçe, Gozde Burgaz, Aytaç G.ürhan Gökçe, Cerium doped glasses containing reducing agent for enhanced luminescence, J. Lumin. 222 (2020) 117175.

[56] J. Bei, G. Qian, X. Liang, S. Yuan, Y. Yang, G. Chen, Optical properties of Ce^{3+} doped oxide glasses and correlation with optical basicity, Mater. Res. Bull. 42 (2007) 1195–1200.

[57] Linyu Pan, Juliana K.M.F. Daguano, Neilo M. Trindadef, Mayara Cerruti, Edgar D. Zanotto, Luiz G. Jacobsohn, Scintillation, luminescence and optical properties of Ce-doped borosilicate glasses, Opt. Mater. 104 (2020) 109847.

[58] M.G. Dong, R. El-Mallawany, M.I. Sayyed, H.O. Tekin, Shielding properties of 80TeO2–5TiO2–(15–x) WO3–xAnOm glasses using Win XCom and MCNP5 code, Radiat. Phys. Chem. 141 (2017) 172–178.

[59] G. Pal Singh, D.P. Singh, Effect of WO_3 on structural and optical properties ofCeO_2–PbO–B_2O_3 glasses, Phys. B 406 (2011) 640–644.

[60] G. Pal Singh, D.P. Singh, Spectroscopic study of ZnO doped CeO_2–PbO–B_2O_3 glasses, Phys. B 406 (2011) 3402–3405.

[61] G. Naga Raju, P. Venkateswara Rao, V. Ravi Kumar, Ch Chandrakala, J. Ashok, Study on the influence of TiO_2 on the characteristics of multi component modifier oxide based B_2O_3 glass system, J. Non Cryst. 498 (2018) 309–314.

[62] Yasser Saleh Mustafa Alajerami, Suhairul Hashim, Wan Muhamad Saridan Wan Hassan, Ahmad Termizi Ramli, The effect of titanium oxide on the optical properties of lithium potassium borate glass, J. Mol. Struct. 1026 (2012) 159–167.

[63] M.A. Marzouk, F.H. ElBatal, H.A. ElBatal, Effect of TiO_2 on the optical, structural and crystallization behavior of barium borate glasses, Opt. Mater. 57 (2016) 14–22.

[64] X. Zhu, Q. Li, Origin of optical nonlinearity for PbO, TiO_2, K_2O, and SiO_2 optical glasses, Appl. Phys. Lett. 71 (1997) 867–869.

[65] A.A. boukais, L.D. Bogomolova, A.A. Deshkovskaya, V.A. jachkin, N.A. Krasil nikova, S.A. Prushinsky, O.A. Trul, S.V. Stefanovsky, E.A. Zhilinskaya, EPR of silica and fluoride glasses implanted with titanium and zirconium, Opt. Mater. 19 (2002) 295–306.

[66] G. Murali Krishna, Y. Gandhi, N. Venkatramaiah, R. Venkatesan, N. Veeraiah, Features of the local structural disorder in Li_2O–CaF_2–P_2O_5 glass–ceramics with Cr_2O_3 as nucleating agent, Phys. B 403 (2008) 702–710.

[67] N. Rajya Lakshmi, Sandhya Cole, Influence of TiO_2 ions on spectroscopic properties of oxyfluoride glasses, Mater. Today Proc. 18 (2019) 192–206.

[68] G. Pal Singh, J. Singh, P. Kaur, S. Kaur, D. Arora, R. Kaur, D.P. Singh, Comparison of structural, physical and optical properties of Na_2O–B_2O_3 and Li_2O–B_2O_3 glasses to find an advantageous host for CeO_2 based optical and photonic applications, J. Non Cryst. Solids 546 (2020) 120268.

[69] K. Fajan, N. Kreidle, Stability of lead glasses and polarization of ions, J. Am. Ceram. Soc. 31 (4) (1948) 105–114.

[70] G. Pal Singh, S. Kaur, P. Kaur, S. Kumar, D.P. Singh, Structural and optical properties of WO3–ZnO–PbO–B2O3 glasses, Phys. B Condens. Matter 406 (2011) 1890–1893.

[71] R. Nadjdsheibani, C.A. Hogarth, The optical properties of some borate glasses, J. Mater. Sci. 26 (1991) 429–433.

[72] Jong Youn Choi, Yun-Mo Sung, Kinetic and structural analyses for the formation of anatase nanocrystals in barium titanoborate glasses, J. Alloys Compd. 647 (2015) 1022–1027.

[73] Qiuling Chen, Qingwei Wang, Qiuhua Ma, Hui Wang, Structure, spectra and Faraday rotation in TiO2 doped diamagnetic PbO–Bi_2O_3–B_2O_3 glasses, J. Non Cryst. Solids 464 (2017) 14–22.

[74] A. Pan, A. Ghosh, A new family of lead bismuthate glass with a large transmitting window, J. Non Cryst. Solids 271 (2000) 157–161.

[75] V. Dimitrov, T. Komatsu, An interpretation of optical properties of oxides and oxide glasses in terms of the electronic ion polarizability and average single bond strength, J. Univ. Chem. Technol. Metall. 45 (3) (2010) 219–250.

[76] X. Zhao, X. Wang, H. Lin, Z. Wang, A new approach to estimate refractive index, electronic polarizability, and optical basicity of binary oxide glasses, Phys. B Condens. Matter 403 (2008) 2450–2460.

[77] M. Abdel-Baki, F.A. Abdel-Wahab, Fouad El-Diasty, One-photon band gap engineering of borate glass doped with ZnO for photonics applications, J. Appl. Phys. 111 (7) (2012) 073506.

[78] E.I. Kamitsos, M.A. Karakassides, G.D. Chryssikos, Vibrational spectra of magnesium-sodium-borate glasses. 2. Raman and mid-infrared investigation of the network structure, J. Phys. Chem. 91 (5) (1987) 1073–1079.

[79] J. Krogh-Moe, The structure of vitreous and liquid boron oxide, J. Non Cryst. Solids 1 (1969) 269–284.

[80] G. Venkateswara Rao, P. Yadagiri Reddy, N. Veeraiah, Thermoluminescence studies on Li_2O–CaF_2–B_2O_3 glasses doped with manganese ions, Mater. Lett. 57 (2002) 403–408.

[81] V.N. Sigaev, P. Pernice, A. Aronne, O.V. Akimova, S. Stefanovich, A. Scaglione, $KTiOPO_4$ precipitation from potassium titanium phosphate glasses, producing second harmonic generation, J. Non Cryst. Solids 292 (2001) 59–69.

[82] P. Nageswara Rao, C. Laxmi Kanth, D. Krishna Rao, N. Veeraiah, Influence of titanium ions on optical properties of AF–PbO–B_2O_3 glasses, J. Quant. Spectrosc. Radiat. Transf. 95 (2005) 373–386.

[83] V.N. Sigaev, I. Gregora, P. Pernice, B. Champagnon, E.N. Smelyanskaya, P.D. Sarkisov, Structure of lead germanate glasses by Raman spectroscopy, J. Non Cryst. Solids 279 (2–3) (2001) 136–144.

[84] A. Dahshan, Yasser B. Saddeek, K.A. Aly, K.H.S. Shaaban, Modather F. Hussein, Ahmed O. Abo El Naga, S.A. Shaban, S.O. Mahmoud, Preparation and characterization of $Li_2B_4O_7$– TiO_2–SiO_2 glasses doped with metal-organic framework derived nano-porous Cr_2O_3, J. Non Cryst. Solids 508 (2019) 51–61.

[85] D.P. Singh, G. Pal Singh, Conversion of covalent to ionic behavior of Fe_2O_3–CeO_2–PbO–B_2O_3 glasses for ionic and photonic application, J. Alloys Compd. 546 (2013) 224–228.

[86] A. Makishima, J.D. Mackenzie, Direct calculation of Young's modulus of glass, J. Non Cryst. Solids 12 (1973) 35–45.

[87] M. Yamane, J.D. Mackenzie, Vicker's Hardness of Glass, J. Non Cryst. Solids 15 (1974) 153–164.

[88] S. Inaba, S. Oda, K. Morinaga, Heat capacity of oxide glasses at high temperature region, J. Non Cryst. Solids 325 (2003) 258–266.

[89] S. Inaba, S. Todaka, Y. Ohta, K. Morinaga, Equation for estimating the young's Modulus, shear modulus and vickers hardness of alumino silicate glasses, J. Jpn. Inst. Met. 64 (2000) 177–183.

[90] A. Pönitzsch, M. Nofz, L. Wondraczek, J. Deubener, Bulk elastic properties, hardness and fatigue of calcium aluminosilicate glasses in the intermediate-silica range, J. Non Cryst. Solids 434 (2016) 1–12.

[91] Kenji Shinozaki, Tsuyoshi Honma, Takayuki Komatsu, Elastic properties and Vickers hardness of optically transparent glass–ceramics with fresnoite Ba2TiSi2O8 nanocrystals, Mater. Res. Bull. 46 (2011) 922–928.

[92] Erdem Şakar, Özgür F.ırat Özpolat, B.ünyamin Alım, M.I. Sayyed, Murat Kurudirek, Phy-X/PSD: development of a user friendly online software for calculation of parameters relevant to radiation shielding and dosimetry, Radiat. Phys. Chem. 166 (2020) 108496.

[93] A. Aşkın, Evaluation of the radiation shielding capabilities of the Na_2B4O_7–SiO_2–MoO_3–Dy_2O_3 glass quaternary using Geant4 simulation code and Phy-X/PSD database, Ceram. Int. 46 (2020) 9096–9102.

[94] I.I. Bashter, Calculation of radiation attenuation coefficients for shielding concretes, Ann. Nucl. Energy 24 (1997) 1389–1401.

[95] ⟨http://www.schott.com/advanced_optics/english/products/opticalmaterials/special-materials/radiation-shielding-glasses/index.html⟩.

[96] G. Pal Singh, J. Singh, P. Kaur, S. Kaur, D. Arora, R. Kaur, K. Kaur, D.P. Singh, Analysis of enhancement in gamma ray shielding proficiency by adding WO3 in Al2O3–PbO–B2O3 glasses using Phy-X/PSD, J. Mater. Res. Technol. 9 (6) (2020) 14425–14442.

[97] S. Stalin, D.K. Gaikwad, M.S. Al-Buriahi, C. Srinivasu, S.A. Ahmed, H.O. Tekin, S. Rahman, Influence of Bi2O3/WO3 substitution on the optical, mechanical, chemical durability and gamma ray shielding properties of lithium-borate glasses, Ceram. Int. 47 (4) (2021) 5286–5299.

[98] V.P. Singh, N.M. Badiger, N. Chanthima, J. Kaewkhao, Evaluation of gamma-ray exposure buildup factors and neutron shielding for bismuth borosilicate glasses, Radiat. Phys. Chem. 98 (2014) 14–21.

[99] D.K. Gaikwad, Shamsan S. Obaid, M.I. Sayyed, R.R. Bhosale, V.V. Awasarmol, Ashok Kumar, M.D. Shirsat, P.P. Pawar, Comparative study of gamma ray shielding competence of WO3–TeO2–PbO glass system to different glasses and concretes, Mater. Chem. Phys. 213 (2018) 508–517.

[100] V.P. Singh, N.M. Badiger, Comprehensive study of energy absorption and exposure buildup factor for concrete shielding in photon energy range

0.015–15 MeV upto 40 mfp penetration depth: dependency of density, chemical element, photon energy, Int. J. Nucl. Energy Sci. Technol. 7 (2012) 75–99.
[101] U. Perişanoğlu, H.O. Tekin, A.S. Abouhaswa, E. Kavaz, Structural and nuclear shielding qualities of B2O3–PbO–Li2O glass system with different Ag_2O substitution ratios, Radiat. Phys. Chem. 179 (2021) 109262.
[102] B. Alshahrani, I.O. Olarinoye, C. Mutuwong, C. Sriwunkum, H.A. Yakout, H.O. Tekin, M.S. Al-Buriahi, Amorphous alloys with high Fe content for radiation shielding applications, Radiat. Phys. Chem. 183 (2021) 109386.
[103] I.O. Olarinoye, F.I. El-Agawany, A. El-Adawy, Y.S. Rammah, Mechanical features, alpha particles, photon, proton, and neutron interaction parameters of TeO2–V2O3–MoO3 semiconductor glasses, Ceram. Int. 46 (14) (2020) 23134–23144.
[104] G. Susoy, E.A. Guclu, O. Kilicoglu, M. Kamislioglu, M.S. Al-Buriahi, M.M. Abuzaid, H.O. Tekin, The impact of Cr2O3 additive on nuclear radiation shielding properties of LiF–SrO–B2O3 glass system, Mater. Chem. Phys. 242 (2020) 122481.
[105] B. Oto, E. Kavaz, H. Durak, A. Aras, Z. Madak, Effect of addition of molybdenum on photon and fast neutron radiation shielding properties in ceramics, Ceram. Int. 45 (17) (2019) 23681–23689.
[106] M. Kamislioglu, E.A. Guclu, H.O. Tekin, Comparative evaluation of nuclear radiation shielding properties of x TeO2+(100–x) Li2O glass system, Appl. Phys. A 126 (2) (2020) 1–16.
[107] G. Lakshminarayana, M.G. Dong, M.S. Al-Buriahi, Ashok Kumar, Dong-Eun Lee, Jonghun Yoon, Taejoon Park, B2O3–Bi2O3–TeO2–BaO and TeO2–Bi2O3–BaO glass systems: a comparative assessment of gamma-ray and fast and thermal neutron attenuation aspects, Appl. Phys. A 126 (3) (2020) 1–18.
[108] V.F. Sears, Neutron scattering lengths and cross sections, Neutron N. 3 (3) (1992) 26–37.